UC Riverside

UC Riverside Electronic Theses and Dissertations

Title

Towards Minimizing the Environmental Impacts of Fossil Energy: Oil-Sorbent Materials and Next-Generation Lithium Ion Batteries

Permalink

https://escholarship.org/uc/item/8bx1s4z1

Author

Patino, Daisy

Publication Date

2019

Copyright Information

Peer reviewed|Thesis/dissertation

UNIVERSITY OF CALIFORNIA
RIVERSIDE

Towards Minimizing the Environmental Impacts of Fossil Energy: Oil-Sorbent Materials
and Next-Generation Lithium Ion Batteries

A Dissertation submitted in partial satisfaction
of the requirements for the degree of

Doctor of Philosophy

in

Materials Science and Engineering

by

Daisy Patino

March 2019

Dissertation Committee:
    Professor Cengiz Ozkan, Co-Chairperson
    Professor Mihri Ozkan, Co-Chairperson
    Professor Kambiz Vafai
    Professor Marko Princevac

The Dissertation of Daisy Patino is approved:

_____

_____

_____
                                                                      Co-Chairperson

_____
                                                                      Co-Chairperson

University of California, Riverside

Acknowledgments

I am greatful for my researchers advisors who supported my graduate studies from the time I was an undergraduate student at UCR. I am also greatful for my committee members who also served as mentors during undergraduate career and contributed to my interest to pursue a higher education. Next, I am thankful to my dear colleagues, friends, and mentors Dr. Hamed Hosseini Bay, Dr. Rachel Ye, Dr. Jeffrey Bell, for introducing me to the fields of materials science, and electrochemistry. I also strongly appreciate the encouragement, guidance, and technical support from my friends and colleagues Dr. Fabian Villalobos, Steven Herrera, Bo Dong, Taner Zerrin, Yige Li, Arash Mirjalili. I will always cherish the bonds we developed during my last year of graudate studies.

The text of this dissertation, in part, is a reprint of the material as it appears in "Scalable Multifunctional Ultra-thin Graphite Sponge: Free-standing, Superporous, Superhydrophobic, Oleophilic Architecture with Ferromagnetic Properties for Environmental Cleaning" Scientific Reports 2016 (Chapter 2), "Advanced Sulfur-Silicon Full Cell Architecture for Lithium-Ion Batteries" Nature Scientific Reports 2017 (Chapter 3), and "Plateau Targeted Conditioning: An Additive-Free Approach Towards Robust SEI Formation in Li-S Batteries for Enhanced Capacity and Cycle life" Nano Energy 2018 (Chapter 3). The co-author Cengiz Ozkan and Mihri Ozkan listed in that publication directed and supervised the research which forms the basis for this dissertation.

To the greatest high school physics teacher, Gabriel Saldana, for inspiring me to

pursue a career in engineering. Thank you. And to my loving partner, Jaime; and

my family, Alfonso & Melissa for always supporting me, reminding me of my

successes thus far, and cheering me on to pursue my dreams.

I love you all.

ABSTRACT OF THE DISSERTATION

Towards Minimizing the Environmental Impacts of Fossil Energy: Oil-Sorbent Materials
and Next-Generation Lithium Ion Batteries

by

Daisy Patino

Doctor of Philosophy, Graduate Program in Materials Science and Engineering
University of California, Riverside, March 2019
Professor Cengiz Ozkan, Co-Chairperson
Professor Mihri Ozkan, Co-Chairperson

The fossil energy industry has caused drastic environmental impacts which have inspired researchers to develop sustainable technologies that can minimize those impacts. Here we explore two types of sustainable technologies: the first aims to directly mitigate environmental impacts after they have occurred, the second aims to prevent environmental impacts by replacing fossil energy sources.

First, we explore the application of a carbon sponge in oil recovery from water. With sustainability in mind, the sponge is derived from sucrose and is synthesized via a facile and scalable three-step process. The sponge offers versatility in absorption properties; both bulk and pulverized forms are capable of absorbing contaminants of various densities. Moreover, the sponge was engineered to be multi functional via minor modifications to the structure.

Next, we explore the sponge's application in next-generation lithium ion batteries as a power source to replace fossil energy. Due to market demands for high performing

batteries, we take a minimalist approach towards materials-research and focus our investigations on the understudied applied-research areas which can help accelerate commercialization of lithium-sulfur technologies. This involves the exploration of scalable production methods such as large scale optimization of slurry densities, a redesign of full cell architectures, and cell operation investigations towards stable interfacial chemistries on the cathode and anode of lithium-sulfur batteries.

Contents

List of Figures

Chapter 1

Introduction

1.1 Fossil Energy and Drawbacks

Fossil fuels have dominated global industries for energy systems throughout vastly changing centuries. Fossil energy may have begun as a spark for the industrial revolution, yet it quickly grew to inspire the momentum towards new consumer technologies that are an integral part of modern society. However, the fruits of modern technology have aided us in identifying the shortcomings of fossil energy within the industrial sector. The life cycle for oil industry includes several stages: mining, transportation, refining, and consumption. Each of these stages contribute to the global ground and air pollution that are inspiring new technologies to combat our dependence on fossil energy [69, 127, 151, 24, 122].

1.2 Technologies for Mitigating Environmental Impacts

For simplicity, we will focus on efforts to reduce environmental impacts in marine oil spills. Current technologies implemented for the task include dispersants, booms & skimmers, in situ burning, and absorbents. Dispersants consists of a surfactant which reduces the surface tension between oil and water, thus leaving behind finely dispersed oil droplets that can be more easily collected or degraded by other methods. However, the application of dispersants has limitations for example, the formula to be cautious to not create a mixture of dispersant and emulsified oil that is more toxic than oil itself [136, 73]. Booms are used to control the areal spread of oil spills, and concentrate it in dense form so that it will be easier for collecting or burning. However, its effectiveness is hindered by waves higher than 11.5 metres and tides faster than one knot per hour [69, 121]. Lastly, burning is typically used in conjunction with boomers and is considered as an emergency response method since air pollution from smoke, smoke particulates can have acute respiratory effects if the burn is near residential areas [69, 16].

Hence, researchers has been encouraged to develop new and novel oil sorbent materials[54, 53, 20, 187, 157]. Owing to their high surface to volume ratio, very low density and desirable electrical properties as well as chemical and mechanical stability, three dimensional (3-D) graphene-based architectures such as foams, sponges and aerogels have been considered as multifunctional viable candidates for oil absorbing materials [97, 154].

1.3 Technologies Aimed to replace Fossil Energy Sources

Mitigation alone is not a viable remedy towards globally reducing the impacts of fossil energy, nor does it address the issue of limited energy sources. In response, there has been national incentives to encourage the production of renewable energy sources that can both slowly reduce the adverse effects of fossil fuels, and provide a naturally and continually replenishable energy. Solar and wind energy are have garnered the most attention in recent years owing to their advantages in sustainability [139, 48, 161, 115].

However, renewable energies need to be dispatchable; lithium ion batteries (LiBs) have been widely adopted for this purpose and for replacing fossil fuels in consumer vehicles. The driving mechanism for LiBs is the intercalation of lithium ions through the active materials within the electrodes. Each battery contains a negative electrode, the anode, and a positive electrode, the cathode. Commercial LiBs typically use graphite as the anode, and a transition metal oxide, such as lithium cobalt oxide ($LiCoO_2$) or lithium nickle manganese cobalt oxide (NMC) as the cathode. Although LiBs are the power source of choice for consumer electronics and electric vehicles, market demands for cost reduction and improved performance exceed the capabilities of current LiB technologies [155, 142, 36].

Accordingly, researchers have turned towards next generation battery materials to procure cheaper, higher capacity batteries [191, 51, 33, 197, 152, 111]. One of the primary materials under consideration for next generation of LiBs is sulfur. Sulfur is a high capacity, energy dense, and abundant cathode material with a theoretical capacity of 1675 mAh/g and energy density of 2600 Wh/kg. However, lithium-sulfur's (Li-S) electrochemistry presents several challenges that inhibit it from being commercialized. Li-S batteries face three major

challenges: detrimental volumetric changes, poor electrical conductivity, and polysulfide shuttling [17, 124, 21]. An 80% volume change mechanically expands and contracts the electrode, degrading its structure and conductive network with each cycle. To prevent mechanical pummeling in sulfur electrodes, researchers have proposed using the structures engineered with void spaces [114] The engineered void spaces accommodate expansion of sulfur while reducing the overall volumetric energy density of the cell. Sulfurs poor electrical conductivity requires extensive carbon additives to achieve practical current rates greater than C/10 or 1.675 mAh/g. Various carbon hosts in the form of carbon nanotubes (CNTs), graphene, reduced graphene oxide (rGO), and other assorted highly conductive carbons have been implemented to help combat poor conductivity of Li-S batteries [91, 129, 153, 71]. However, excess additives decrease an electrodes sulfur content and create dead weight in the electrode. This limits the cells potential energy density, making it impractical for industry.

Polysulfide shuttling in Li-S results from the long chain polysulfides (Li_2S_8 - Li_2S_4) being highly soluble in ether electrolytes, which are commonly used in Li-S batteries due to their preferred high ionic conductivity. Once (Li_2S_8 - Li_2S_4) dissolves in the ether electrolyte, polysulfides shuttle from the sulfur electrode across the separator collecting on the counter electrode (lithium metal). These polysulfides form an insulating layer during delithiation, reducing ionic conductivity and causing capacity loss [117, 167]. To suppress polysulfide shuttling, several groups have employed various thin films or core shell structures such as graphene paper and pomegranate like carbon structures [29, 100, 8, 114]. These structures trap polysulfides within the cathode, and improve performance. However, the methods utilized to achieve this are impractical for commercialization.

Chapter 2

Multifunctional Technologies: Carbon Sponge for Oil-Spill Recovery & Energy Storage

2.1 Overview

Carbon foams are composed of a cluster of carbon atoms webbed together in a free-standing three dimensional porous network. Depending on the specific allotrope of carbon and thus the resulting key physical properties such as surface area, porosity, conductivity, and mechanical integrity, carbon foams have been developed for various applications including gas sensing [188] and adsorption [137], biological applications [92], thermal management [132], radiation shielding [31], and energy storage [137, 109, 181]. In particular, the low density and high surface area to volume ratio of carbon foams make them attractive candidates for oil recovery applications [154, 61, 14]. It is imperative for such a candidate however, to have a low affinity to water and a high oil absorption capacity [37]. In this regard, static contact angle measurements are employed to measure the hydrophobicity of carbon foams; wherein, a surface is hydrophobic when its static water contact angle is greater than 90°. Likewise, a contact angle of or greater than 150°is considered superhydrophobic. Accordingly, researchers have implemented various secondary methods to improve these properties via means of chemical etching and carbon nanotube growth [44, 97] in addition to the base methods for fabricating foams which in often involve hydrothermal reduction and assembly of graphene oxide sheets [97, 108, 180]. In effect, the water repellency of foams reach superhydrophobicity yet the overall process requires high control over experimental conditions,and is not scalable as the end product is often limited to a single application.

2.2　Sponge Development

To combat the complexity of effective foams, we developed a practical synthesis method for a superhydrophobic foam, reffered to simply as "Sponge", capable of serving multiple functions including oil recovery and energy storage. The sponge is a free standing structure with exceptional surface area and porosity that can easily be tailored per desired application. One particular advantage of the sponge, is that it does not require an additional chemical activation treatment to enhance the surface area or porosity; the developed sponge has multimodal porosity including macro, meso and micropores. The sponge and synthesis process have been thought out to be practical, inexpensive, and scalable.

2.2.1　*Synthesis Process*

Sponge is synthesized via a simple three step process involving just three precursors (Fig 2.1). First, equal molar amount of sucrose and polyvinyl alcohol (PVA) are mixed with iron nitrate (Fe_3O_3) in a 4:1 ratio within an aqueous solution (sol). As the aqueous solution of the precursors stirs at 90°C, nitric acid droplets are added to reach a solution pH of 3 and to initiate the polymerization. The heated mixture forms a resin (gel) within a few hours and is then dried in a vacuum oven at 120 °C to extract excess moisture and nitrogen compounds, and to initiate porosity upon expansion of the resin (step 2). Lastly, the dried resin is annealed at (500°-1000 °C) under argon and hydrogen gas to induce growth of graphite sheets and nucleation of nanoparticels.
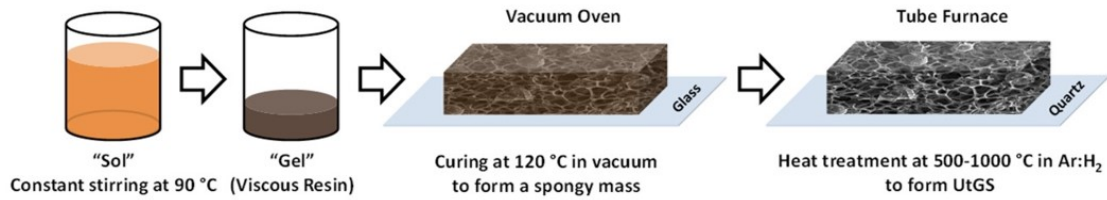
Figure 2.1: Illustration of the sol-gel synthesis method for Sponge.

2.2.2 *Morphology Characterization*

Figure 2.2.a reveals the microstructure of the sponge which appears to be a maze of interconnected macropores. Higher magnification SEM (Fig 2.2.b) shows that the surface of the sponge seems to be very porous and may be considered as possible connected meso-pores and channels. TEM images reveal that sponge is consisted of convoluted graphitic sheets as well as dispersed iron nanoparticles (Fig 2.2.c). Higher magnification TEM imaging demonstrates that iron nanoparticles are encapsulated within the structure by few layers of graphene (Fig 2.2.d). HRTEM images show interplanar distances of 0.34 nm which corresponds to the stacking of sp2-hybridized layers of carbon (Fig 2.2.d inset). As pointed out in Figure 2.2.e, the structure seems to comprise numerous minuscule graphene domains and randomly oriented flakes which attain a rough microstructure encompassing microchannels. HRTEM image resolved from the surface of the sponge indicates the existence of very small graphene-based domains with random orientation and complex stacking as well as sub-nanometer channels separating them (Fig 2.2.f).

In this sense, the width of the microchannels separating the graphene domains seems to deviate slightly from the measured interplanar distance of 0.34 nm. Moreover, measured interplanar spacing of the stacked layers appeared to conform to that of graphitic structures[132].
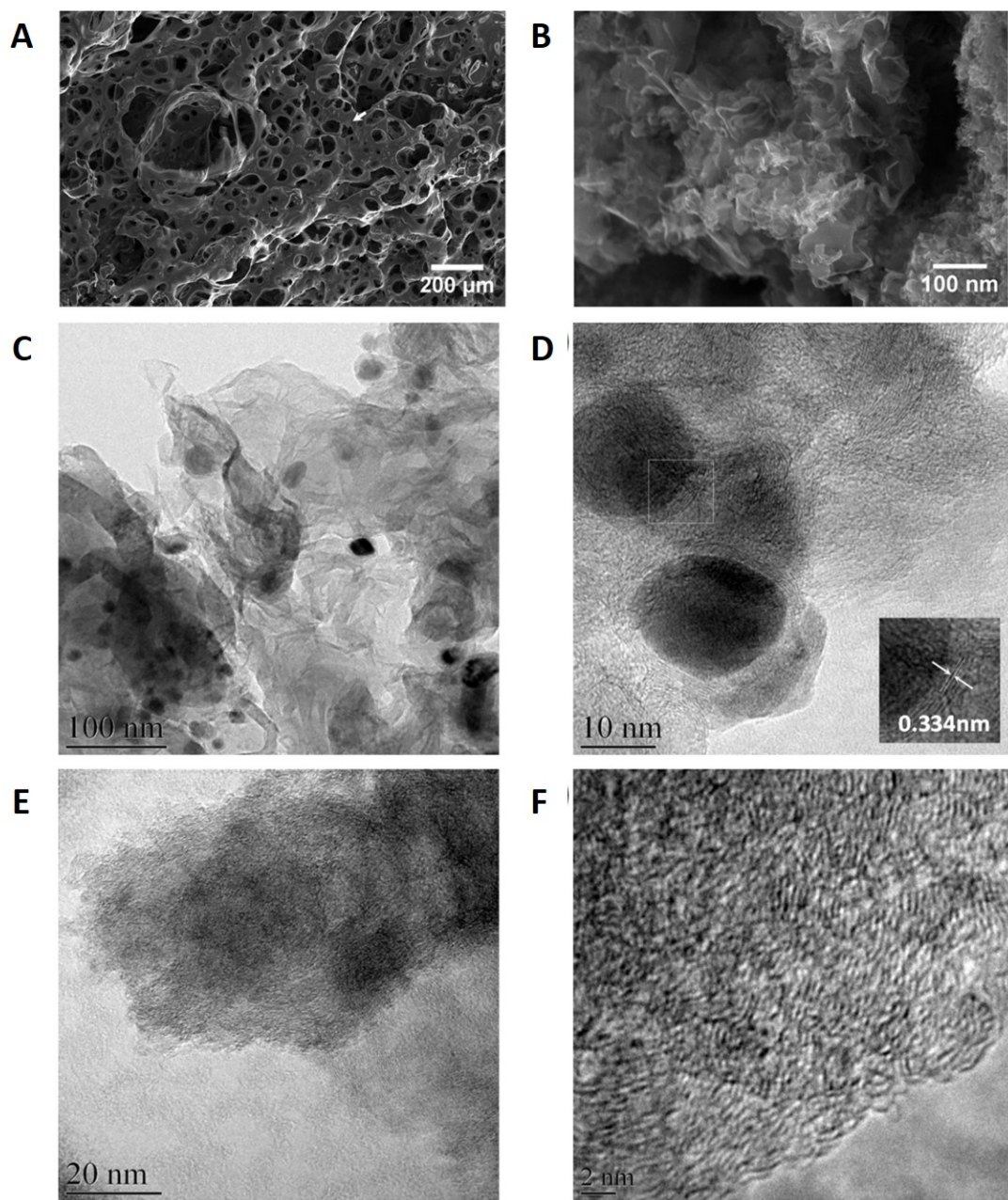
Figure 2.2: SEM image of the sponge microstructure. (b) High magnification SEM image acquired from the surface of the sponge roughly where the white arrow is pointing at. (c)) Low magnification TEM image of Sponge (d) High magnification image of the Fe nanoparticles encapsulated in graphene-based sheets (inset: HRTEM image showing the graphene layers with the interplanar distance highlighted). (e) Low magnification image around the surface of sponge. (f) HRTEM image showing the microstructure of the surface of Sponge.

2.2.3 *Porosity & Surface Area*

BrunauerEmmettTeller (BET) surface area measurements have been carried out to quantify the surface area and porosity of sponge architecture. Figure 2.3.b,c summarize the results of adsorption-desorption isotherms and BET pore size distribution, respectively. It seems that the structure exhibits a combination of type I and type IV N2 adsorption-desorption isotherms [120, 147]. The adsorption in relative pressures less than about 0.1 implies that micropors or microchannels can be found in the sample, whereas the hysteresis loop from relative pressures of about 0.5 to 1.0 is related to the mesopores [190]. The average pore diameter was calculated using DFT model to be about 1.4 nm. The Langmuir and BET surface area of sponge sample were measured to be 1356.30 and 823.77 m^2g^{-1}, respectively which implies that there is no predominant concern for chemical activation in order to enhance porosity and surface area. Besides, the density of sponge was calculated to be $0.017\,gcm^{-3}$. It may be inferred that the majority of the surface area should be attributed to the micropores and microchannels. Nonetheless, this cannot contradict the actuality and contribution of the mesopores which can be identified in high magnification SEM image. While the mesopores may contain a portion of the total volume of the condensate, the amount of micropores and microchannels significantly prevails. Thus mesopores do not contribute to the pore distribution as might be expected [6].

2.2.4 *Chemical Characterization*

X-ray Diffraction (XRD) and Raman spectroscopy were carried out on sponge samples prepared at different temperatures To characterize the details of the microstruc-
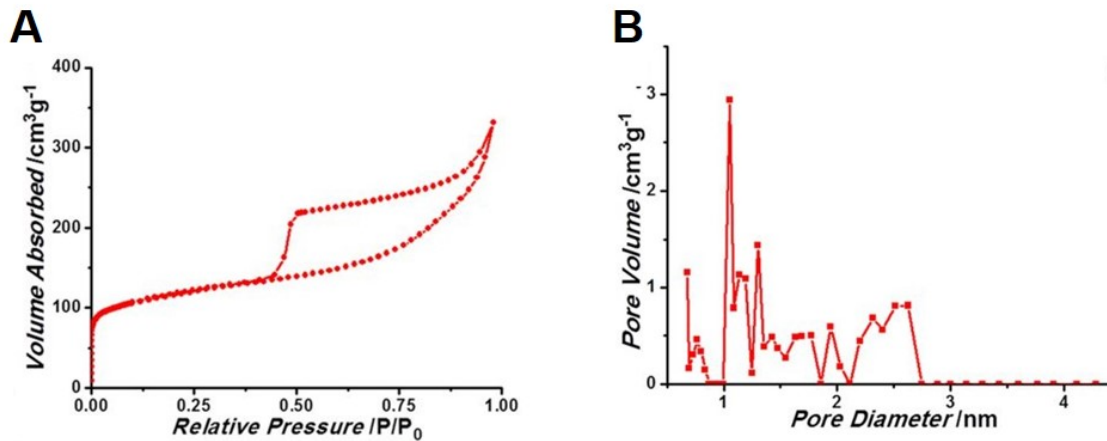
Figure 2.3: a) BET surface area measurement of sponge with I and IV type N2 sorption. b) Pore size distribution of sponge.

ture and overlook the structural changes and phase evolution. XRD patterns of sponge samples heat treated at 500°- 1000 °C are demonstrated and compared in Figure 2.4.a. According to characteristic diffraction angles, sp2-hybridized layers in form of graphene as well as α-Fe [172] and Fe_3O_4 [131] can be identified at different temperatures. The peak at 24°may correspond to (002) reflection and the peak at 43°can link to superposition of (101) and (100) reflections in sp2-hybridized graphitic lattice structure[179]. It has been reported by other researchers that these two peaks can be related to graphene sheets and flakes[28, 49, 50, 199]. In addition, syntheses at higher temperatures yield to higher crystallinity of the structure since the XRD peaks appear to be sharper with higher relative intensities. As seen in Figure 2.2.c,d, it is most likely that the dispersed nanoparticles in the microstructure are α-Fe nanoparticles with diameter of about 20 nm. While some of these nanoparticles are encapsulated with few layers of graphene, some nanoparticles can be found unprotected on the surface of the sponge. It is critical to note that the final heat treatment of the sponge precursor is done under argon and hydrogen atmosphere which

12
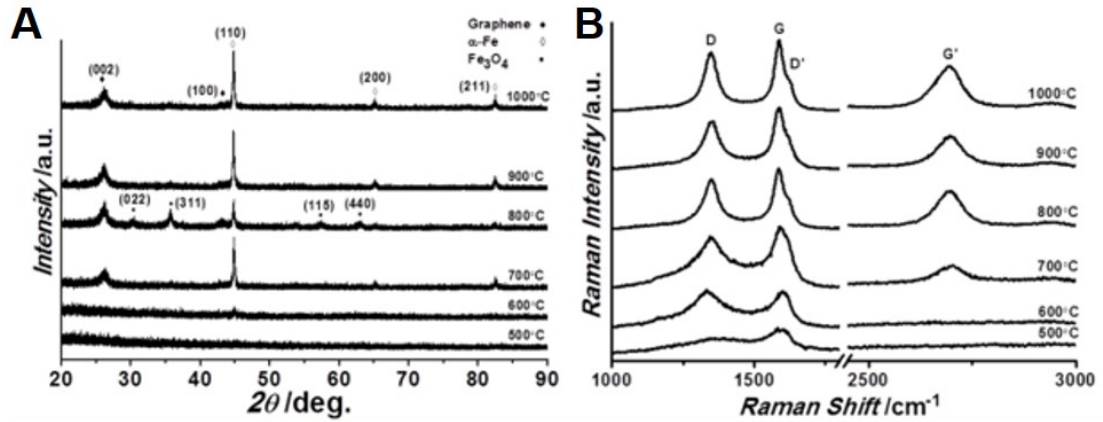
Figure 2.4: a) XRD plots of sponge heat treated at different temperatures. b) Raman spectra plots of sponge heat treated at different temperatures.

prevents the oxidation of Fe nanoparticles. Nevertheless, as soon as the sponge is removed from the reducing environment of the furnace and subjected to air, the nanoparticles are highly prone to surface oxidation. Consequently, trace of Fe_3O_4 is observed in the XRD pattern from 700°C (Fig 2.4.a).

Figure 2.4.b shows Raman spectra of sponge heat treated at different temperatures. Three characteristic Raman peaks of graphene, D, G and G', respectively at 1335, 1580 and 2680 cm-1 can be observed in the spectra [57]. Since G' peak of graphite is believed to be asymmetric and split into four peaks [56, 58], the peak centered at about 2680 cm-1 can be associated to G' peak of graphene. The broad D peak in the spectra infers the high level of disorder in structure. To investigate the changes in the sponge structure, D to G (ID/IG) and G' to G (IG'/IG) peak intensity ratio at different heat treatment temperatures have been plotted separately. As the temperature ramps up, ID/IG which refers to the disorder in graphene layers, follows a general ascending trend except from 600 °C to 700 °C, where

13

it plummets. Similarly, IG'/IG as a measure for the number of stacked graphene layers, increases with temperature. It seems that the formation of graphene-based sheets starts at about 700 °C, since G' peak emerges at this temperature. Evolution of the system from 600 °C to 700 °C can be interpreted as incubation for amorphous to crystalline transition. Since the graphene-based sheets are starting to nucleate and grow, the degree of disorder seems to drop temporarily. Afterwards, the formation of the spatially convoluted graphene sheets yields to higher degree of disorder. The ascending trend of IG'/IG implies that the growing graphene layers are not stacking or possibly forming a turbostratic structure, where the stacked layers are slipped sideways relative to one another to create micro-channels [18]. The presence of D' peak at 1608 cm^{-1}, accentuates high degree of disorder in graphene domains and also convey that graphene-based sheets may have been doped with nitrogen [110].

2.3 Sponge for Oil Recovery

2.3.1 *Hydrophobicity and Oleophilicity*

Figure 2.5.a represents the contact angle measurement of water on the sponge which was evaluated to be 154.72°. Such an exceptional hydrophobicity is a result of numerous microscopic and nanoscopic voids of air and surface roughness at the interface with water as well as the possible absence of hydrophilic groups on the surface of the sponge. To investigate the uptake behavior of sponge structure with time, a sample was exposed to compressor oil, and its weight change was monitored over the course of one minute (Fig 2.5b). The oil was absorbed into the sponge upon contact, and in about 4 to 6 seconds

14

the maximum absorption was reached. To enumerate the absorption capacity (c=15.57) of sponge, the mass change after oil uptake (mf=327 mg) is divided by the initial mass (mi=21 mg) of the sponge. As a result, the maximum weight of compressor oil that can be absorbed by sponge is about 15.57 times of its weight. Meanwhile, sponge manifested a similar trend for ethanol sorption, displaying an absorption capacity of 22.69. Figure 2.5.c shows snapshots of spreading and absorption behavior of compressor oil in contact with sponge surface, acquired at 60 millisecond intervals. It reveals that the sponge is oleophilic since the oil is penetrated into the structure upon contact and completely absorbed by the sponge in about 300 ms.

Sponge offers micro-, meso- and macro-pores at the same time and the high intrinsic surface area of sponge can be attributed mostly to the meso- and micro-pores. These pores and channels may not contribute to oil absorption due to surface tension restriction of oil which could explain the setback in oil absorption capacity of sponge compared to carbon nanofiber, carbon nanotube and graphene aerogels. Alternatively, this setback can be compensated by the facile fabrication process, multi-functionality and scalability of sponge.

2.3.2 *Sponge Sustainability*

To put the recyclability of sponge to test, a sample was soaked with toluene and then subjected to a flame. The sample containing the absorbed toluene was combusted until all of toluene was consumed. The fire was self-extinguished due to the absence of fuel, and the sponge sample remained intact and could be used again. Similar studies have been carried out to demonstrate the fire-resistivity and recyclability of graphene-based sponges
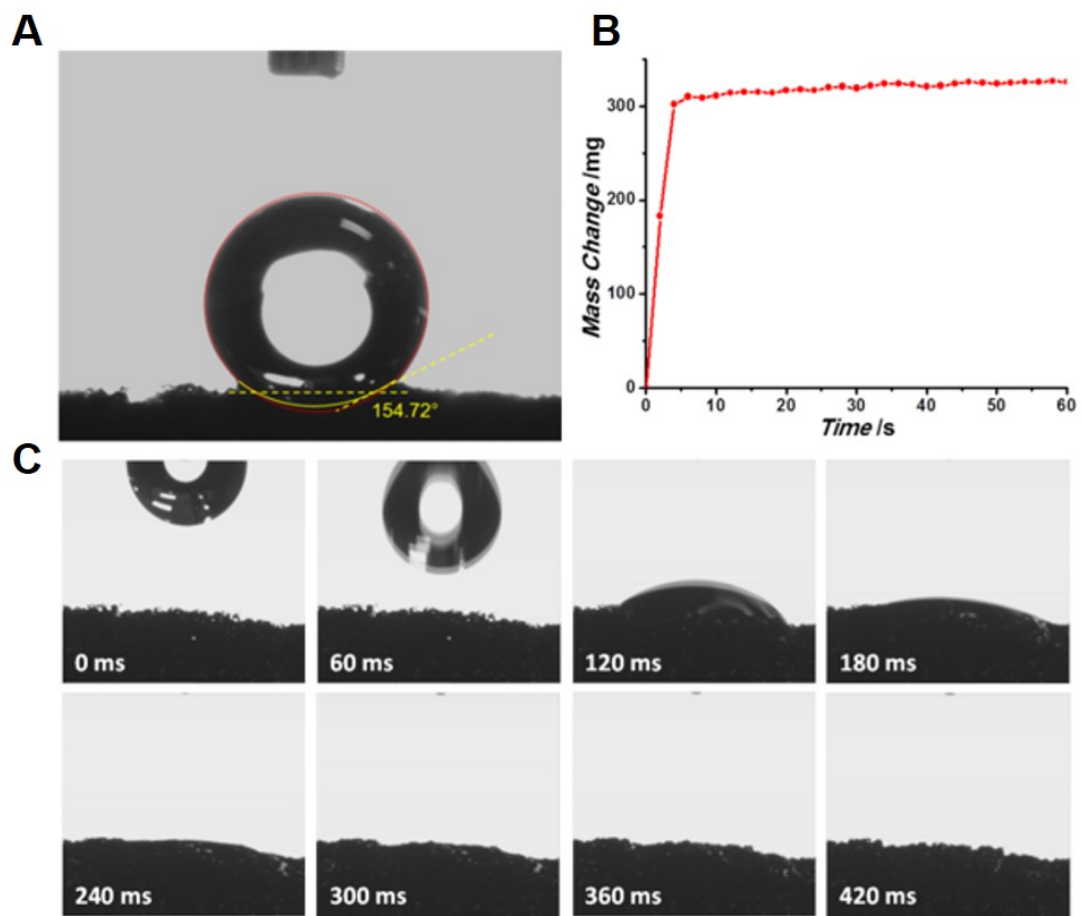
Figure 2.5: a) Contact angle measurement of sponge showing super-hydrophobicity. b) Rate of oil uptake for sponge. c) snapshots of oil absorption on sponge surface

[133, 198]. However, the recovery of the absorbates such as oil and organic solvents from the sorbent after uptake remains a priority. A simple process can be implemented to heat up the sponge with the contained absorbate to evaporate the absorbed contaminant. The vapor can then be condensed to liquid form and recycled [174]. To further quantify the cyclic recovery, the weight changes of a sponge sample has been evaluated. In this instance, the sample was saturated with ethanol and the ethanol was evaporated by annealing at 500°C for 30 min. Sponge dry weight was consistent within 10 cycles and was measured to be 20.78 mg. Sponge post saturation weight was 469.8 to 471.2 mg and no evident decrease in absorption capacity was observed.

2.4   Sponge for Energy Storage

Inspired by the incentives to reduce the adverse impacts from fossil energy, and to reduce our dependence on it, we wanted to test the multi-functionality of the sponge in the field of energy storage. As stated previously, a core area of research for next-generation lithium-sulfur cathodes is the mitigation of polysulfide shuttling via entrapment in a porous carbon host. Hence, we hypothesize the mesoporosity of sponge can be a suitable candidate for trapping polysulfides.

2.4.1   *Synthesis of Sponge-Sulfur Cathodes*

Prior to preparing sponge-sulfur cathodes, iron nanoparticles were etched via hydrochloric acid (HCl) treatment on bulk sponge samples. As a result of acid treatment, the amount of Fe in the structure was decreased from 12.69 to 5.55 wt% by dissolving the

unprotected Fe nanoparticles. Therefore, about 5.55 wt% of the structure is believed to be graphene wrapped α-Fe nanoparticles. Next, powdered sponge and elemental sulfur were combined in a heated dimethyl sulfoxide solution to prepare the active material for the electrodes. For details, see electrode synthesis methods in the following chapter.

2.4.2   *Results and Discussion*

Cyclic Voltammetry (CV) is a electrochemical technique commonly used to study the reduction and oxidation processes of molecular species; wherein, the current peaks observed indicate redox reactions signature to the electrode material. CV measures current generated by the battery in response to an applied potential. When sulfur electrodes are cycled by CV, the reduction of sulfur causes current to increase, forming cathodic peaks as observed in the bottom profiles for CV Figures 2.6.a,c which are read from right to left. As the surface layer of sulfur is reduced, lithium ions diffuse through to continue reducing the entire electrode, thus causing the peak current to drop (typically to -.3 mA). The two cathodic peaks observed indicate the reduction of sulfur to long chain polysulfides (starting at 2.4 V), followed by further reduction to form short chain polysulfides and solid lithium sulfide (starting at 2 V). In general, an electrode with better ionic conductivity will reduce surface material faster, thus causing the cathodic peak to shift upward in potential (to the right along the x-axis).

After the reduction process is completed, the potential-scan direction is reversed to initiate oxidation of lithium sulfide (read from left to right at the top of CV profiles). Oxidation profiles for sulfur electrodes under CV typically show one signature anodic peak corresponding to the re-formation of elemental sulfur. Overall, an electrode with a greater

A

Current (mA)

0.6
0.4
0.2
0
-0.2
-0.4
-0.6

1.6   1.8   2   2.2   2.4   2.6   2.8   3

Ecell (V)

30% Sulfur

C

Current (mA)

Ecell (V)

58.4% Sulfur

B

Specific Capacity (mAh/g)

1000
900
800
700
600
500
400
300
200
100
0

0   5   10   15   20   25   30

Cycle Number

D

Specific Capacity (mAh/g)

1200
1000
800
600
400
200
0

0   1   2   3   4   5   6   7

Cycle Number

956.82   884.54   702.01   748.86   705.17   528.16
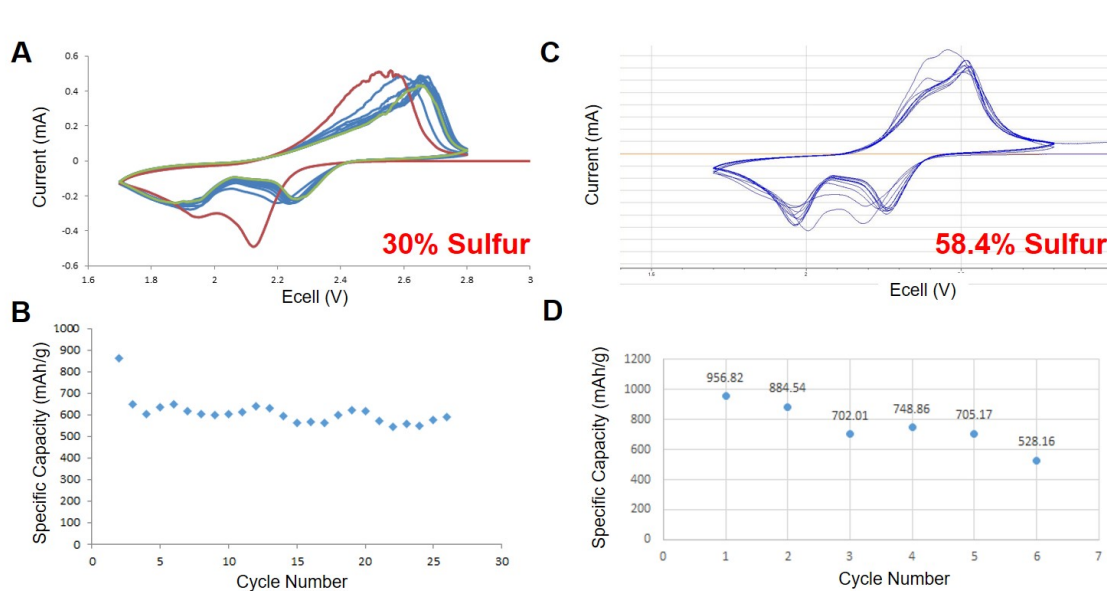
Figure 2.6: a) Cyclic Voltammetry of a preliminary sponge-sulfur cathode displaying unwanted side reactions. b) Specific capacity corresponding to the preliminary sponge-sulfur cathode. c) Cyclic Voltammetry of a new sponge-sulfur cathode displaying stable reactions. d) Specific capacity corresponding to the preliminary sponge-sulfur cathode

quantity of active material (sulfur) will yield greater peak intensities.

Figure 2.6.a shows the initial CV for preliminary sponge-sulfur electrodes. The noise observed in the anodic spectrum are indicative of unwanted side reactions between sulfur and residual iron nanoparticles depicted 2.2.c,d. However, the specific capacity for this battery is comparable to that in literature, approximately 600 mAhg^{-1}, despite the limited life cycle for the battery. Therefore, it was expected that a thorough etching treatment would remove all traces of Fe nano particles and improve the performance of the sponge-sulfur cells. CV analysis for the new sponge-sulfur battery in Fig 2.6.c depict smoother profiles, indicating only the signature redox reaction for sulfur batteries, and reassuring that all Fe particles have been removed. It is inferred that the resulting weight reduc-

tion enabled higher weight loading of sulfur, as quantified by thermogravimetric analysis (58.4 wt% vs 30 wt% of sulfur). The cathodic peaks show higher intensity than those for the battery in Fig 2.6.a, reconfirming the higher sulfur loading. Additionally, the anodic curves reveal more of the oxidation transition from lithium sulfide first to polysulfides, and ultimately to sulfur. However, specific capacity for this battery is significantly affected the removal of Fe nanoparticles. It is proposed that the removal of graphene-wrapped Fe nanoparticles effectively destructed the graphitic properties of the sponge, leaving behind mostly amorphous carbon with minimal crystallinity in comparison to graphite. The lack in crystallinity disables intercalation lithium ions into the carbon host, thereby impairing the available capacity as seen in Fig 2.6.d.

2.5   Highlights

Mitigating the environmental impacts of fossil fuel industries is a primary motive towards developing novel materials for sustainable applications. Here we present a practical synthesis method for a carbon sponge derived from sucrose. The sponge displays exceptional hydrophobicity with a contact angle of 154.72 °against water, as well as oleophilic properties; thus, making it a viable candidate for oil recovery in industrial spills. The application of sponge can be extended to broader water decontamination applications, as it is also capable of absorbing liquid contaminants of various densities. Furthermore, minor modifications to the sponge enable a proof of concept for its use in energy storage. Although sponge is an attractive host for sulfur electrodes, owing to both their advantages in sustainability, there is a need for an in-depth understanding of the working mechanism in Li-S batteries including

lithium ion intercalation, and redox reactions upon cycling. It is recommended to approach this task with commercially available materials to minimize the complexity of characterizing new electrode material systems. The following chapter provides a comprehensive study of sulfur electrodes and explores their applications in full cell battery architectures.

Chapter 3

Applied-Research Tools for Expediting Next-Generation Technologies: Sulfur-Silicon Batteries

3.1 Overview

Lithium-ion batteries (LiBs) have been replacing power sources for numerous applications in recent years. The momentum for this trend is not expected to decline given the unique advantages in energy density for LiBs relative to other rechargeable batteries. Beyond consumer electronics, LiBs will continue to shift global sectors of transportation and grid storage for renewable energies as society becomes more invested in reducing our dependence on fossil energy. Despite the bright future for LiBs, two critical issues need to be addressed: performance and safety. Performance is especially important for transportation applications, whereas electric vehicles need to compete with combustion engines in order to meet national incentives to reduce carbon emissions in the atmosphere. Safety is at the forefront for LiB research as concerns of battery fires are most hazardous in congested scenarios as in commercial airlines.

Therefore, research into LiBs should go beyond finding the highest capacity from a given material system. Research should focus on understanding the key failure mechanisms signature to specific battery chemistries in effort to develop *safe* LiBs for next generation technologies. Here we go beyond the standard materials-research approach and explore how practical electrochemical characterization techniques can be used in parallel to cell operation techniques to retrieve more information about the driving and failing mechanisms in lithium-sulfur batteries.

3.2 Conventional Electrochemical Characterization Tools

The theoretical capacity of a new electrode material is the primary motivator for researchers who seek to develop next-generation batteries. However the real amount of electric charge that a battery can provide, measured in units of Amp-hour (Ah), is contingent on variables including ambient temperature, rate of charge/discharge, and various cell parameters such as weight. Accordingly, galvanostatic (constant current) cycling of a new electrode material is the first experiment a researcher will conduct in pursuit of interpreting its performance. Galvanostatic cycling can be performed at various charge/discharge rates to generate potential vs. time plots (Fig 3.1) which can be used to calculate a cell's experimental capacity in response to a controlled variable. Wherein, the most common control variable is the current rate (C-rate) at which a cell is cycled, and is calculated relative to the cell's theoretical capacity. For example, a lithium cobalt oxide ($LiCoO_2$) electrode with a theoretical capacity of 140 mAhg^{-1} cycled at C-rate of 1C will take one hour for 140 Amps to completely discharge or charge all of its capacity. Similarly, if the battery is cycled at C/10, a current of 14 mA is required to fully discharge the battery within ten hours.

Typically a higher C rate will result in a lower experimental capacity that a cell can deliver. This decrease in capacity is observed as shortened voltage plateaus in galvanostatic plots, as depicted in regions A-D in Fig 3.1. Thus, capacity dependence on C-rates is a common use of galvanostatic plots. However it is not very insightful in regard to the mechanisms that fail upon high C-rates which contribute to the lower capacity. Here we explore a combination of electrochemical techniques in a manner which can be more insightful to failure mechanisms.
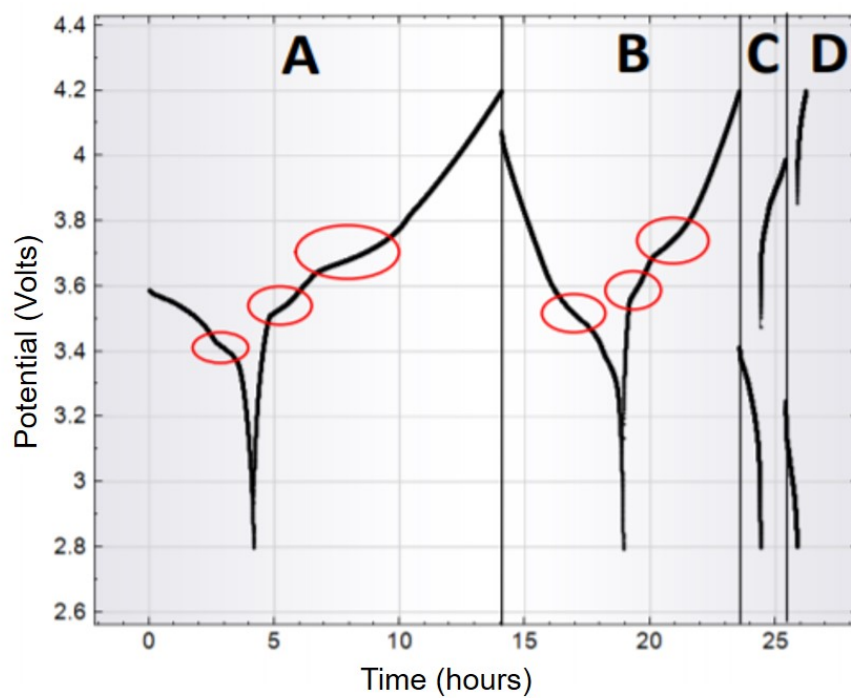
Figure 3.1: Conventional Galvanostatic Cycling with Potential Limits for lithium ion batteries.

The galvanostatic intermittent titration technique (GITT) is an electroanalytical tool commonly used in lithium ion technologies which uses transient and steady state measurements to obtain kinetic and thermodynamic properties of electrodes materials. The GITT procedure applies short current pulses to a cell, followed by rest periods until a desired equilibrium potential limit is reached. This causes causes equilibrium voltages to rebound from the applied current; the time stamp between these two potentials are used to calculate diffusivity coefficients for the electrode via the following expression:

$$D = \frac{4}{\pi}\left(\frac{L^2}{\tau}\right)\left(\frac{\Delta E_{Relax}}{\Delta E_{Pulse}}\right)^2 \tag{3.1}$$

Wherein, L is the diffusion length of the electrode, τ is the time duration of the pulse current, ΔE_{Relax} is the change of equilibrium voltages at the end of two sequential open-circuit rest periods, ΔE_{Pulse} is the change in the cell voltage during the current pulse. For an in depth explanation of GITT analysis, readers are recommended to read [146, 201].

In conventional lithium ion cells, current pulses induce concentration changes within the host electrodes. In lithium sulfur batteries however, the concentration change occurs within the electrolyte due to the reduction of sulfur to electrolyte-soluble polysulfides. Hence, it is a complex procedure to quantify values such as the chemical diffusivity coefficient of lithium ions and the resistivity through the electrolyte in lithium sulfur cells, as opposed to conventional solid state lithium ion cells. Accordingly, research efforts to utilize GITT for lithium sulfur cells, omit the polysulfide shuttle mechanism to obtain a semi-solid state model. Herein, we explore GITT analysis in a qualitative manner to enable a complete lithium sulfur model to depict lithium diffusivity despite the polysulfide shuttle effect.

26

3.3 Understanding Li Ion Mobility in Response to Electrode Loading

An increase in consumer demands for longer lasting and better performing batteries has turned researchers towards sulfur and silicon electrodes as next-generation lithium ion batteries. A majority of LiB research focuses on optimizing the chemical composition of these electrodes to yield improvements in capacity and longevity of batteries. However, the benefits from experimental variables which alter chemical compositions are often constrained to strict conditions such as specific materials compatibility. Here we explore a universal approach towards improving the performance of sulfur and silicon electrodes that does not interfere nor rely on specific materials synthesis processes. Specifically, we want to investigate the effects slurry density in half cells via a practical processing technique. Calendering tools are used in various fields to tailor the density of a deposited material on a substrate. In this case, we use a calender machine to vary the packing density of sulfur and silicon slurries on the current collectors for half cell batteries.

3.3.1 *Electrode synthesis*

The sulfur cathode was made with 20 wt% Poly(acrylic acid) (PAA, 1800 g/mol, Sigma-Aldrich) and 80% wt% acetylene black sulfur composite(ABS). The aforementioned ABS was made by dissolving 200 mg of Sulfur (S, 99.998% trace metals basis, Sigma-Aldrich) in 20 ml of Dimethyl Sulfoxide (DMSO, Fisher Chemical) at 90 C, heated by a heating jacket (Brisk Heat). 129 mg of Acetylene black (Alfa aesar, 50% compressed) was then added to the solution, the solution was stirred for 3 hours before the heating jacket was

removed and the solution was allowed to cool while stirring. The resulting ABS composite was then washed by anhydrous ethanol (Decon Labs, Inc.) several times to ensure the removal of DMSO and dried at 60C for 24 hours. To make the sulfur electrode, Poly(acrylic acid) (Sigma Aldrich, 450,000) and ABS were mixed with 1-Methyl-2-pyrrolidinone (NMP, Sigma-Aldrich) and then casted on a large piece of aluminum chip (Alfa Aesar, 0.025mm thickness, 99.45% purity) by a doctor blade (MTI Automatic Thick Film Coater, BYK Doctor Blade). The casted electrode sheet was then dried in a convection oven (Cole-Parmer, Stable Temp) at 60C for 24 hours. The silicon electrode was made with 40 wt% of commercial silicon (GNM Silicon nanoparticles 80nm), 25 wt% Acetylene black (Alfa aesar, 50% compressed), and 35 wt% Poly (acrylic acid) (Sigma Aldrich, 450,000). The materials were mixed and sonicated in ethanol and then casted on a large copper chip (Alfa Aesar, 0.025mm thickness, 99.8% purity) with a doctor blade (BYK) and was then dried at 60C for 24 hours.

3.3.2   *Slurry Density Processing*

Slurry-casted electrode sheets are passed through a calender machine (IRM) which compress the sheets between two rollers at varying settings denoted by the gap spacing between the rollers. The calender settings are shown Figure 3.2. Individual coin shaped electrodes are then cut out of the post-calendered sheets to assemble coin cell batteries.

Calendaring Gap	Material Loading	Si Density (mg/cm^3)	Sulfur Density (mg/cm^3)
30 um	S, Si (2.4-2.5 mg/cm^2)	481	483
40 um	S, Si (2.4-2.5 mg/cm^2)	471	463
50 um	S, Si (2.4-2.5 mg/cm^2)	461	419
60 um	S, Si (2.4-2.5 mg/cm^2)	440	405
70 um	S, Si (2.4-2.5 mg/cm^2)	425	380

Figure 3.2: Various calender settings for altering the densities of slurry loadings: silicon and sulfur.

3.3.3 Results and Discussion

Standard galvanostatic cycling discussed earlier was used to calculate and plot the specific capacities per cycle, as shown in Figure 3.3a,b. At a glance, it is clear that a calender setting of 40 μm yields the highest capacity for sulfur half cells. However, a clear conclusion cannot be drawn directly from the capacities for silicon half cells. A setting of 50 μm appears to yield the best capacity momentarily between cycles 30-80, yet a setting of 40 μm prevails at the end of cycling. Additionally, the 30 μm setting shows irregular capacity fluctuations which cannot be explained for by galvanostatic cycling alone. Hence, we utilize GITT to further interpret the chemical interactions occurring in the batteries.

GITT uses a series of current pulses, each followed by a relaxation period. Herein, electrodes were pulsed at C/50 for 10 minutes, immediately followed by 10 minutes rests.

This interval was repeated until complete discharge. Oscillations in the voltage profile represent changes between the pulsed voltages and steady state voltages [40]. Shorter oscillations throughout the voltage profile are ideal, indicating minimal voltage excitation during the relaxation period; this represents a homogeneous material reduction and improved lithium diffusivity. However, small oscillations may also be indicative of poor material access to the conductive network [130]. Ideally, ionic diffusivity in Li-S batteries should remain consistent throughout cycling. Consistency in diffusivity indicates steady active material utilization, minimal polysulfide shuttling, and electrode mechanical stability. The continuing changes in diffusivity results from active material loss, mechanical changes in the electrodes, decreased material participation, or changes in the concentration of polysulfides in the electrolyte.

Figures 3.3.c,d reveal that the improved capacity from 40 μm calendering stems from improved diffusivity of lithium ions through the densified electrode. The tight packing of sulfur slurry enables better mechanical integrity of the electrode which is better equipped to withstand volumetric expansion upon cycling. Likewise, the loosest density packing resulting from 70 μm calender gap permits voids in the electrode during cycling which interfere with lithium intercalation, thus impeding lithium ion diffusivity.
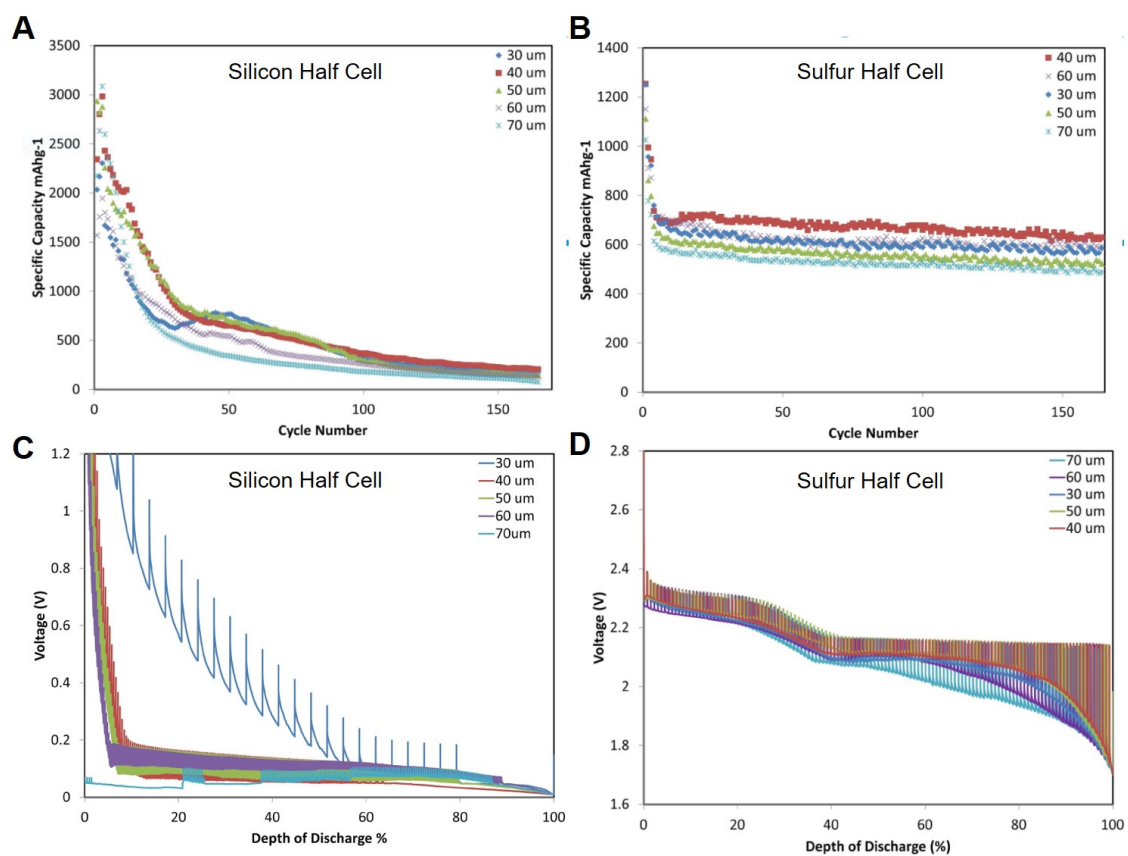
Figure 3.3: a) Multiplot of specific capacities for silicon half cells with different slurry densities. b) Multiplot of specific capacities for sulfur half cells with different slurry densities. c) Multiplot of GITT profiles for silicon half cells with different slurry densities. d) Multiplot of GITT profiles for sulfur half cells with different slurry densities.

GITT profiles for the silicon half cell provide more insights into the capacity fluctuation for 30 μm in 3.3.a. The elongated discharge plateaus for 30 μm in 3.3.c represent severe fracturing in the silicon electrode which inhibit uniform current densities upon cycling and cause localized short circuits. Furthermore, a comparison of GITT profiles for 40 and 50 μm setting for silicon reveal that 40μm maintains steady kinetics throughout the discharge cycle, which coincides with the least capacity fading found in 3.3.a.

3.4   Redesigning Sulfur-Silicon Full Cell Architectures

Half cell research is great tool for optimizing individual next-generation electrodes. However, in order for electrodes to be deemed as viable technologies, they need to be tested in the full-cell format with a limited amount of lithium. Conventional full-cells rely on the cathode as the source of lithium ions; for example, NMC (Lithium Nickle Cobalt Managanese Oxide) cathodes are commonly paired with graphite anodes to complete a full-cell. Per this principal, the lithiated form of sulfur cathodes (lithium sulfide) should be paird with a compatible anode to complete a full-cell. However, processing of lithium sulfide is prone to releasing hydrogen sulfide gas which is poisonous, corrosive, and flammable [185, 64, 104]. In effort to reduce hazards and promote scalability, researchers seek alternatives to a prelithiated sulfur full-cells. Here we pair sulfur cathodes with silicon anodes in a novel battery architecture which bypasses the challenges of prelithiated materials.

3.4.1 *Methods*

A full cell using sulfur and silicon electrodes is attractive for several reasons. Sulfur and silicon are environmentally benign and abundant. Furthermore, the theoretical energy density of a sulfur silicon full-cell (SSFCs) is 1982 Wh/kg, far exceeding the theoretical energy density of current LiBs while only potentially costing \$13/kWh. This presents a great advantage over commercial NMC-graphite batteries which peak at a theoretical energy density of 605 Wh/kg, and cost approximately \$180/kWh.

Electrodes for SSFCs were constructed using a facile process. Shown in Figure 3.4, the silicon electrode is patterned to create an access point for the lithium chip to make contact with the current collector. The access point allows the silicon slurry and lithium chip to act as one electrode, creating a complete circuit, allowing current to travel through the lithium. The patterned silicon electrode is engineered to only expose a small surface area of the current collector, thereby maximizing silicon slurry loading, causing only a small area of the lithium chip to make direct contact with the current collector. Each SSFC requires roughly 6.44 mg of lithium, accounting for the lithiation of sulfur and silicon, along with SEI lithium consumption. To ensure enough lithium is available in the system, each cell is loaded with 8 mg of lithium. Lithium not making direct contact with the current collector (non-participating lithium) requires repeated cycling to slowly integrate lithium ions into the system. A schematic of the constructed SSFCs is shown in Figure 3.4.
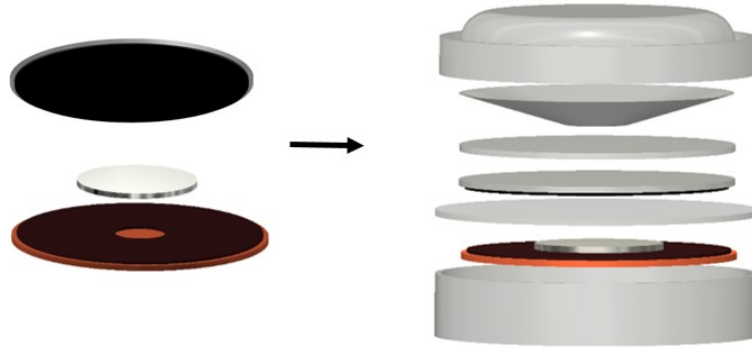
Figure 3.4: Novel full-cell architecture with a lithium chip integrated on a patterned silicon anode

3.4.2 **Results and Discussion**

Figure 3.5.c shows galvanostatic cycling for the SSFC. The initial energy density of the SSFC is 100 Wh/kg at C/50 then increases to 414 Wh/kg over 10 cycles. The increase in energy density is attributed to the continuous integration of non-participating lithium, shown in Figure 3.5.c. The SSFC has an energy density of 350 Wh/kg for over 250 cycles and a coulombic efficiency of approximately 95%. The fluctuation in coulombic efficiency from cycle 1 to 150 is due to the process of lithium integration. Lithium integration creates a unique chemical reaction in the SSFC. During the charge step in a conventional full-cell, lithium ions from the cathode reacts with the anode. However, in the SSFC, additional lithium ions from the chip react with silicon in the anode, increasing the charge capacity. The coulombic efficiency is calculated as discharge capacity divided by charge capacity. Hence, lithium ions from the chip lower the coulombic efficiency of cycles 1 to 150 despite the cathode operating with a coulombic efficiency of 99%, shown in Figure 3.5.a. By cycle 150 all the required lithium is incorporated in the SSFC and is actively participating in the redox reaction, however, excess lithium remains. During charge, lithium ions from the
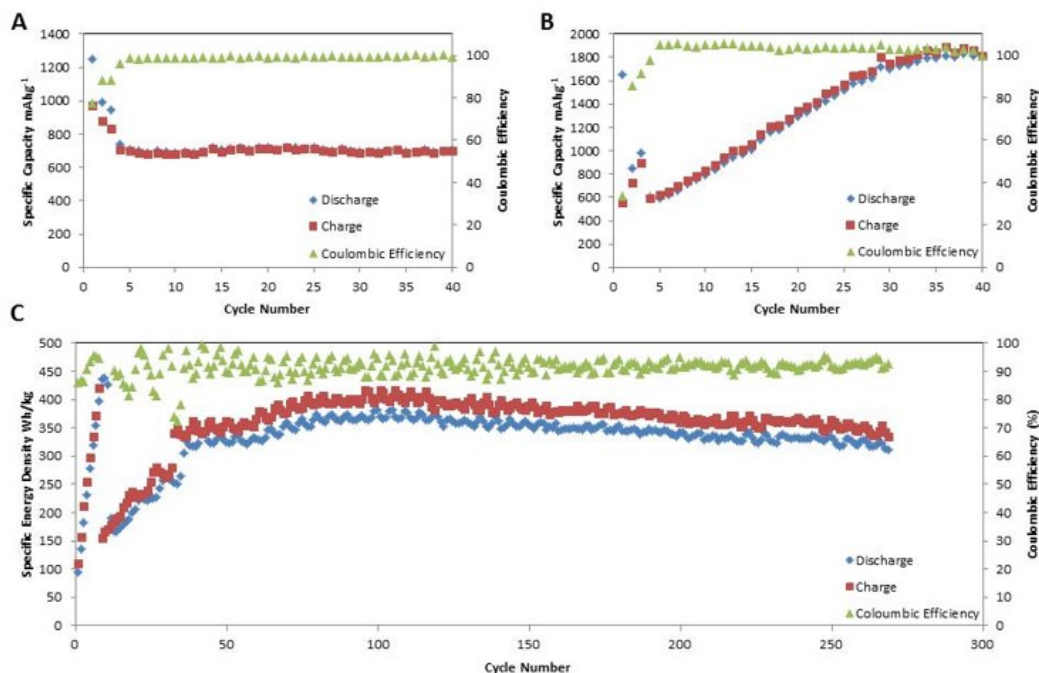
Figure 3.5: Specific capacities and coulombic efficiencies for a) sulfur half cell, b) silicon half cell, c) Sulfur-silicon full cell.

cathode plate onto the excess lithium chip while in parallel, lithium ions from the chip react with silicon which in turn lowers the coulombic efficiency to 95%. Additionally, the wave like fluctuations in capacity shown in Figure 3.5a,b, & c results from temperature changes occurring inside the testing room.

GITT, shown in Figure 3.6, was employed to investigate changes in lithium diffusivity within the individual battery systems[60, 17]. The batteries were subjected to current pulse intervals with a rate of C/50 for 10 minutes, followed by 10 minute rests until complete discharge/charge. In Figure 3.6, the varying thickness of the voltage profiles represent varying lithium diffusivities in the system. Thinner voltage profiles indicate improved diffusivity while thicker voltage profiles represent the inverse [130, 129].

In Figure 3.6A, the profile for the sulfur half-cell displays a slight decrease in voltage plateaus from cycles 1 to 2. This occurrence is also observed in Figure 2A & 3A, and is attributed to the change in ionic and electric conductivity caused by the incremental SEI formation and polysulfide shuttling[17]. As seen in Figure 3.6B, the silicon half-cell experiences a voltage shift within the first two cycles; this is attributed to SEI formation. However, voltage profiles and diffusivity equilibrate by the second cycle, indicating that the silicon half-cell has faster kinetics than the sulfur half-cell. Hence, it is determined that the kinetics of sulfur half-cell is the limiting factor for the diffusivity of the SSFC. Figure 3.6C shows the GITT profile for the SSFC. Figure 3.6C depicts the voltage profiles of the SSFC resembling the sulfur half-cell, revealing plateaus at 2.3 V and 2.1 V after reaching equilibrium. However, the first cycle of the SSFC shows a discharge profile offset from the sulfur half-cell; this is attributed to limited lithium participation in the first cycle. Additionally, the second cycle shows a drastic shift in voltage profiles. The excess voltage plateau in cycle 2, at roughly 50% depth of discharge, alludes to the aforementioned issues associated with the architecture of the cell. The ionic and electric conductivity continue to improve from cycles 10 to 310 due to SEI formation and polysulfide shuttling. Hence, the diffusivity of the system improves, and we observe thinner voltage profiles in the subsequent cycles. The observable change in diffusion in cycle 2 to 10 is a result of total lithium utilization allowable in the system. Again, at this stage, the SSFC does not have access to the majority of required lithium. Hence, the cell requires subsequent cycles to integrate non-participating lithium into the anode. Figure 3.6D compares the diffusivity of SSFC to the sulfur half-cell, wherein we see a notable difference within the early cycles. At 80 -
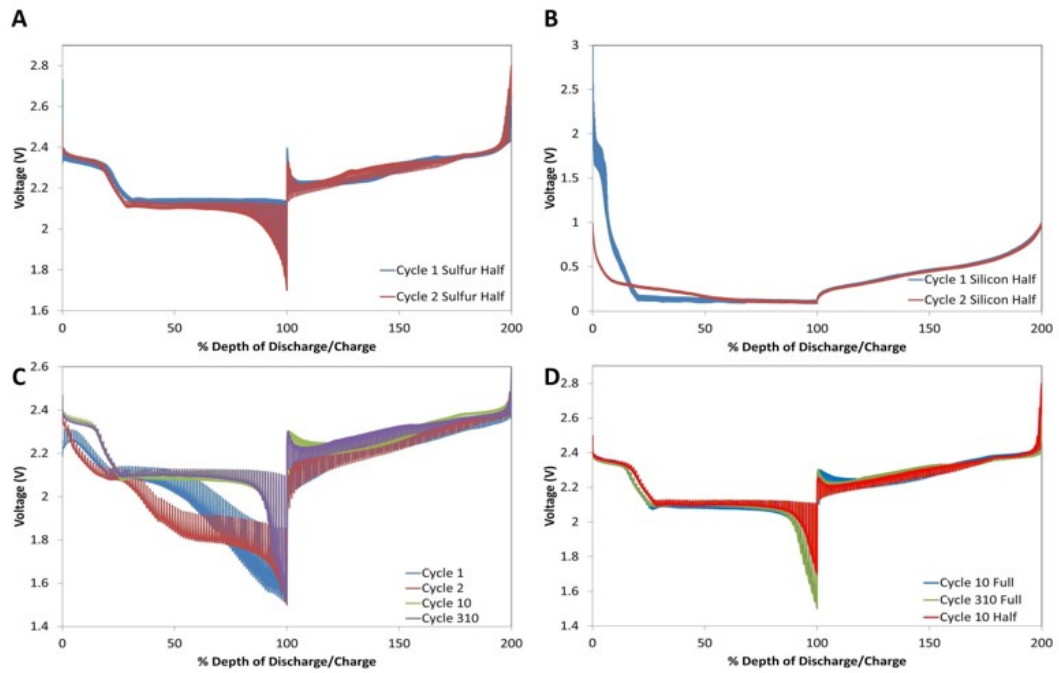
Figure 3.6: GITT profiles for a) sulfur half cell, b) silicon half cell, c) Sulfur-silicon full cell, d) Sulfur-silicon full cell in comparison to the sulfur half cell

100% depth of discharge, the observable difference in diffusivity from the half-cell to SSFC is caused by the charge transfer resistance of the silicon anode. Similarly, once the cell starts to charge, the notable difference in diffusivity profiles at 0-20% depth of charge is a result of charge transfer resistance in the anode for the SSFC. Ultimately, Figure 3.6D depicts the SSFC voltage profile continues to coincide with that of the half-cell once it has developed a complete utilization of lithium.

3.5 Cell Operation Protocols Towards a Reinforced Solid Electrolyte Interface in Lithium-Sulfur Cathodes

Lithium-sulfur (Li-S) is one of the most promising next-generation lithium-ion battery systems due to its high theoretical specific capacity. However, Li-S batteries suffer from a short cycling life, poor mechanical stability and low coulombic efficiency. Developing a robust solid electrolyte interface (SEI) plays a critical role in alleviating these issues. Current approaches for a robust SEI are mostly based on using additives which fall under three categories: reduction type, reaction type, and morphology modifier. However, additive use in Li-S tends to have adverse effects on energy density, internal resistance, and cycling stability while additive-free approaches to robust SEI formation have not garnered enough attention[43, 71]. Herein, we explore an understudied area of LiB research: cell operation effects on working/failure mechanisms of a battery. Specifically, we are interested in characterizing the effects of cyling rates during the formation phase of a battery which aims to prepare an electrode to withstand high-rate cycling. Current formation practice in Li-S research will slowly cycle a cell at steady rates within C/100 - C/20 to allow for the formation of protective surface films as the Solid Electrolyte Interface before current rates are increased to test experimental capacity[175, 123, 99, 100, 126], However, formation practices are seldom understood, yet it has the potential to increase cell performance at little cost regardless of electrode design.

	C-Rate	Voltage Limits	C-Rate	Voltage Limits
Method 1 (datum)	C/50	2.8 V – 1.7 V		
Method 2	C/50	2.8 V- 2.1 V	C/100	2.1 V – 1.7 V

Figure 3.7: Formation methods tested for sulfur half cells.

3.5.1 *Methods*

Herein, we test two formation protocols for a Li-S half-cells. The first protocol, Method 1 applies a constant current rate of C/50 (0.175 mA) during discharge and charge for 3 cycles. This models the common formation practice reported by researchers and thus is used as the datum in this study. Method 2 applies a rate of C/50 during discharge within 2.8 V to 2.1 V and a rate of C/100 (0.0875 mA) during the potential region associated with SEI formation in Li-S batteries, 2.1 V to 1.7 V, as showin in Fig 3.7.

3.5.2 *Results and Discussion*

A comparison of specific capacities for sulfur half cells subject to formation Method 1 and Method 2 is shown in Figure 3.8.a. Both methods show fluctuations in capacity due to temperature changes, it is observed that batteries undergoing condition method 2 fluctuate the least. This results from the stable and high quality SEI layer created during formation [86].

Since all batteries have the same sulfur loading, a higher capacity of 652 mAh/g for Method 2, compared to 612 mAh/g for Method 1 is indicative of more active material

retained during the cycling routine and more material utilization. Active material loss for Method 1 can be a result of poor SEI layer permitting polysulfide shuttling into the electrolyte and the counter electrode, or sulfur detaching from the conductive network during volume expansion/contraction [42]. Additionally, better material utilization for Method 2 can result from a better mechanical structure and SEI layer. A robust SEI layer formed during formation prevents cracking of the SEI layer during high cyclic expansion. This reduces material exposure to the electrolyte and prevents the generation of new and excess SEI. Furthermore, the robust SEI layer creates better mechanical stability and ionic pathways, which further stabilizes battery performance, resulting in 494 mAh/g capacity after the 4 week period of testing. This represents a significant improvement from the battery subject to conventional formation which ends with 444 mAh/g in capacity.

Coulombic efficiency (CE) for both methods measure capacity retention for the batteries, Fig 3.8.b. Large spikes in CE up to 103% (1st, 11st, 21st, and the 31st cycle) represent GITT measurements taken during standard cycling of the batteries. GITT disrupts the CE of the following cycle by overcharging the battery and activating sulfur that does not participate normally due to limitations in the conductive network. As a result, the following cycle has an increased discharge capacity and a CE over 100 %. Method 2 batteries have the highest and most stable CE. A stable CE indicates minimized polysulfide shuttling, consistent conductive pathways, and stability under temperature fluctuations[91] These advantages are consequential from a robust SEI layer.

We propose the robust SEI layer of Method 2 batteries traps polysulfides inside the SEI, causing a minimal amount of polysulfides to travel across the electrolyte and to
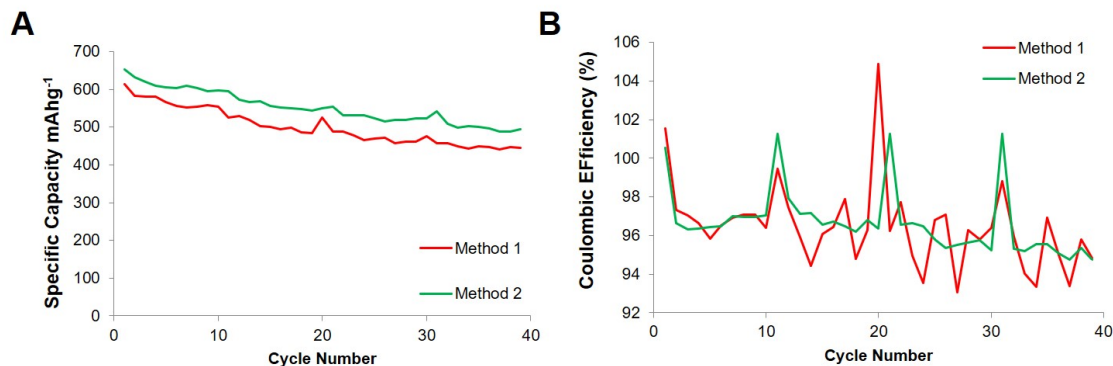
Figure 3.8: a) specific capacities for sulfur half cells subject to formation methods 1 and 2. b) coulombic efficiencies for the corresponding capacities.

the lithium counter electrode. This in turns reduces the damage polysulfides can cause to the lithium SEI while also reducing temperature impact on the electrolyte. This is in good agreement with Fig3.8.a, which show minimized capacity fluctuation in Method 2 batteries.

GITT profiles for the two methods shown in Figure 3.9 appear to indicate better diffusivity for Method 1 batteries during the first week of cycling. Considering that Method 1 batteries lose more capacity, we can infer that a higher amount of polysulfides reside in the electrolyte; this is reported to increase the ionic conductivity of the battery. Hence, during this stage, Method 2 battery experiences slower diffusivity since it lacks the conductivity boost from excess polysulfides. However, at the end of week 3 and 4, Method 2 batterys diffusivity increases and surpasses Method 1 batteries. This is because all batteries experience polysulfide saturation in the electrolyte over time and reach similar ionic conductivity, but Method 2 batterys minimized mechanical degradation due to a robust SEI layer maintained the best electrical conductivity network. The conductive network is the predominant variable contributing to ionic diffusivity at week 4; low coulombic efficiency
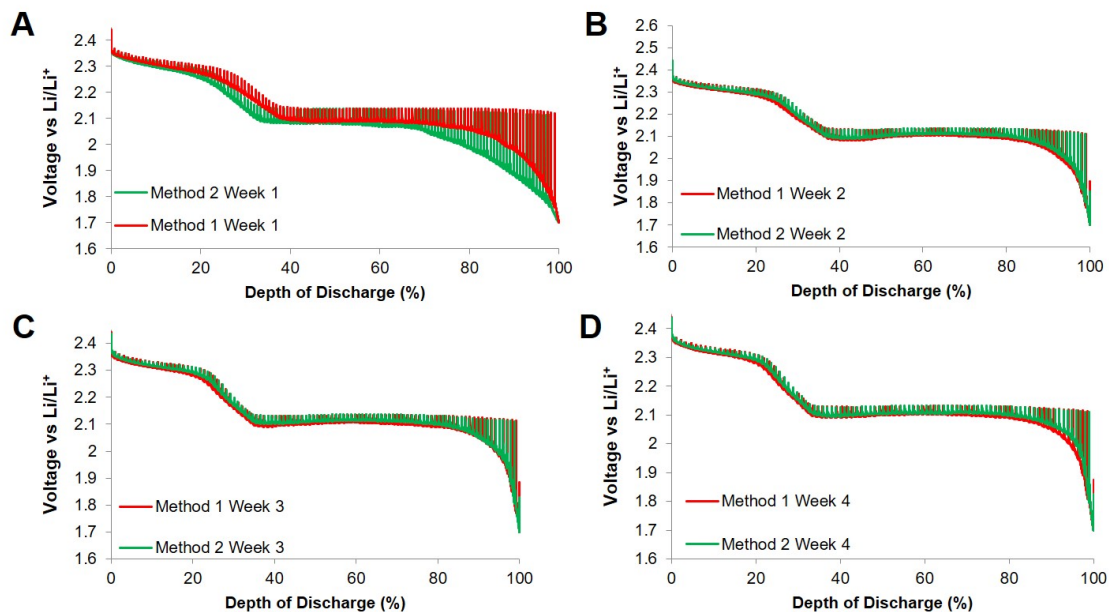
Figure 3.9: GITTs profiles for sulfur half cells measured after week periods of standard galvanostatic cycling.

degradation further supports this conclusion.

Potentiostatic electrochemical impedance spectroscopy (PEIS) is a non-destructive method that characterizes the integrity of the electrode-electrolyte interface, passivation layers, electronic conductivity of electrode material, diffusion of lithium within electrode, and diffusion of lithium-ions in electrolyte near electrode surface [42]. Impedance was measured within frequency bounds of 10 kHz and 10 mHz.

One resistance value quantified by PEIS is the resistance associated with the formation of the SEI layer, Rsei. A higher Rsei indicates more robust SEI layers. Sulfur does not natively form any permanent passivation film similar to SEI layers observed in silicon or carbon electrodes [114]. We propose the SEI resistance observed in the sulfur electrodes mainly originate from the carbon additive, but may also be affected by polysulfides and

electrolyte composition. Similarly, the equivalent series resistance (ESR) represents the total resistance contributed by solution resistance, charge transfer resistance, and contact resistance in the batteries [42]. Figure 3.10.b shows the evolution of ESR for the sulfur half cells.

Rsei for both methods increases during week 1, yet Method 2 batteries spike in Rsei during week 2. This spike can be attributed to delithiated polysulfides; as long chain polysulfides delithiate into sulfur, sulfur particles gather on the conductive network and SEI layer. Sulfur gathering on the SEI layer can be mistaken as a contributing factor to Rsei. As sulfur becomes increasingly densified on the SEI layer with each successive cycle, Rsei increases proportionally, shown in 3.10.a. This phenomenon occurs in both methods during week 1 but only exists for Method 2 batteries in week 2. It can be inferred this stems from a robust SEI layer, which mitigates polysulfide shuttling. It is speculated that amount of surface-sulfur contributes to the mitigation of polysulfide shuttling in Method 2. Once the surface layer of sulfur is lost to polysulfide shuttling, Rsei stops increasing.
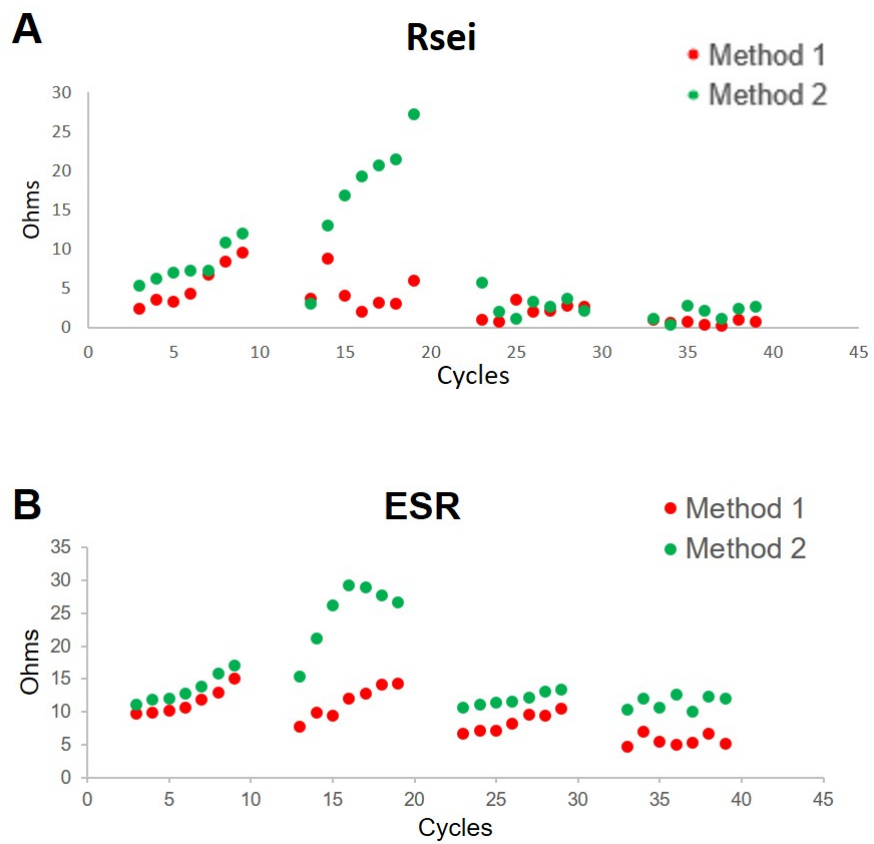
Figure 3.10: PEIS measurements of sulfur half cells during cycling: a) SEI resistance (Rsei) for batteries subject to formation methods 1 and 2. b) Equivalent series resistance (ESR) for batteries subject to formation methods 1 and 2.

ESR increases for both methods increase gradually during week 1, but stabilizes by week 3. In contrast to Methods 1 batteries, ESR for Method 2 battery continue to increase during week 2. ESR is dominated by solution resistance, or electrolyte conductivity, but also takes into account changes in SEI resistance.This relationship is highlighted by the increase in ESR as a consequence to the spike in Rsei during week 2. As suggested by the previous electrochemical techniques, Method 1 experiences a higher rate of polysulfide shuttling which ultimately cause the observed capacity fading in Fig 3.8. The increased quantity of polysuldifes in the electrolyte contribute to ionic conductivity in the cell which effectively lower the ESR values for Method 1.

3.6   Highlights

Optimization of slurry densities is a practical technique that can be implemented on any electrode to retrieve the highest capacity given its slurry chemistry. The universality and of this approach inspires researchers to be mindful of developing scalable laboratory practices that can easily be translatable to commercialization. However, this technique needs to be adequately characterized to confidently define the parameters which attribute to the driving and failing mechanisms in the electrodes. Here we show how GCPL is not sufficient characterization for the task, yet qualitative GITT analysis proved to compliment GCPL in effort to highlight the internal kinetics of the electrodes in repose to different slurry densities. Ultimately, the optimized silicon and sulfur electrodes from this study are used as standards of performance for further experiments as in sulfur-silicon full cells and in investigating the effects of formation rates on SEI integrity in sulfur half cells.
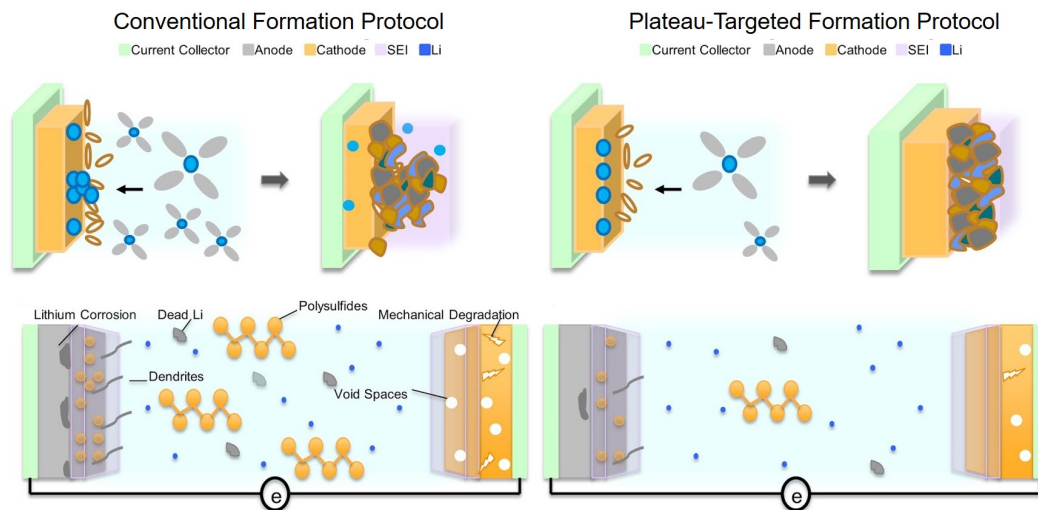
Figure 3.11: Illustration of the electrochemical benefits from the modified formation method presented.

The sulfur-silicon full cell presented herein serves as a simple alternative to pre-lithiated sulfur-silicon full cell systems. An additional benefit from this approach is the facile control over lithium loading to compensate for SEI formation and lithium degradation. As a full cell configuration for next generation lithium ion batteries, the SSFC demonstrates an energy density of 350 Wh/kg over 250 cycles. Furthermore, this is the first time to the best of our knowledge a sulfur silicon full cell has been fully characterized by GITT analysis. The results presented here show that the SSFC is comparable to other prelithiation methods demonstrated in research, while offering advantages in scalability.

Lastly, here we explored the effects of formation protocols on SEI formation in Li-S half cells. It was observed through the testing models, that plateau targeted formation (Method 2) develops robust SEI layers. We propose that this is attributed to the slower formation rates targeting the second discharge plateau of Li-S batteries which allocates more time for steady formation of the SEI layer, while reducing time spent in the first plateau

associated with long chain polysulfides. The resulting SEI layer suppresses the solubility of long chain polysulfides, improves ionic pathways, maintains mechanical integrity, increases capacity, and enhances cycling stability of the Li-S battery. An illustration of these improvements is shown in 3.11. Additionally, this technique bypasses the use of additives and their associated adverse effects. Despite the lack of research centered on formation protocols for next-generation electrodes, this approach can universally be applied to various material systems.

Chapter 4

Beyond Materials-Research: Cell Operation Protocols Towards Dendrite-Suppressing Surface Films on Lithium Metal Anodes

4.1 Overview

Lithium metal electrodes are regarded as the optimal anode for next generation lithium ion batteries. Unfortunately, the lithium metal anode falls subject to several challenges such as dendrite formation and low coulombic efficiency, which inhibit its candidacy as a viable technology. As such, substantial research efforts alter cell parameters in effort to manipulate interfacial chemistries, mitigate dendrite growth, and improve cyclability. Here we demonstrate a practical cell operation approach to reinforce the Solid Electrolyte Interphase in lithium anodes via a modified formation protocol governed by the redox reactions found in Lithium-Sulfur systems. Multiple formation protocols, the galvanostatic procedures for electrochemically preparing a cell to withstand high rate cycling, were applied to Li-Li symmetrical cells to investigate the effects on SEI integrity and dendrite mitigation. Comparative galvanostatic and electrochemical impedance data on cells subject to multiple formation protocols reveal that cell operation during the formation phase plays a critical role on interface stability of lithium metal anodes. Additionally, scanning electron microscopy images demonstrate that minor modifications to formation protocols can significantly minimize destructive lithium plating, as well as the size and dispersion of lithium dendrites. The practicality of this approach deviates from the convention of materials exploration, yet highlights the importance of understanding the nature of interfacial chemistries in response to cell operation. We believe the transferability of this approach has the potential to expedite the commercialization of next-generation lithium ion technologies.

4.2 Challenges with Li Anodes

The implementation of lithium ion technology has grown exponentially in recent years over several markets including electric vehicles, power grids, etc. However, commercial lithium ion technologies cannot meet the growing energy density demands from these markets. Hence, researchers are looking into the next-generation materials that can enable higher performing technologies. Lithium-Sulfur (LiS) batteries have amassed substantial attention as a promising next-generation full cell system. Sulfur is regarded as the optimal cathode owing to its high specific capacity 1675 mAhg^{-1}, high energy density 2600 Whkg^{-1}, and material abundance [167, 34, 138]. Likewise, lithium metal is widely regarded as the optimal next-generation anode, owing to its high theoretical capacity of 3860 mAhg^{-1}, low gravimetric density .59 g/cm^{-3}, and low negative redox potential -3.04 V [22, 101]. The advancement of LiS systems is hindered however by an unbalanced research effort towards optimizing each electrode respectively; one third of research efforts towards LiS systems target to improve on the challenges inherent to lithium metal anodes [178, 22, 38]. Hence it is foreseeable that a shift in attention to the understudied areas of research could accelerate commercialization of next generation technologies like lithium sulfur batteries.

For lithium metal anodes, the critical investigations needed are scalable methods to improve on their high reactivity and excessive volume expansion which lead to poor cyclability and safety hazards. It is expected for electrodes to undergo volume changes during the cycling process. For example, conventional graphite anodes undergo 10% volumetric expansion [22, 200] and sulfur cathodes undergo upto 80% [22, 163]. However, lithium anodes are subject to infinite volume changes [22, 200, 101, 184], and when coupled with their

inherent high reactivity, this poses several self-reinforcing challenges in regard to the SEI layer. Due to the very low electrochemical potential of Li, electrolytes are spontaneously reduced at the surface and develop a mosaic SEI layer with heterogeneous ionic conductivity and nucleation sites[184, 169, 83]. During cycling, changes in the SEI can cause irregularities in ion flux[101, 184]. Wherein cracks in the SEI locally enhance ion flux by exposing fresh Li with a lower energy barrier for ion transport; and accumulated SEI impede ion flux via local blockades for ion transport. Both instances adversely affect the battery by igniting a continuous consumption of lithium and electrolyte, which leads to an increase in cell resistance and ultimately, irreversible capacity fading.

The most notable effect of heterogeneous nucleation sites in the SEI is dendrite formation[165, 144, 103]. During cyclic volume fluctuations, fractures in the SEI can cause dendrites to lose contact with current collector and remain as dead lithium in the electrolyte. This in effect, crowds the mobility of lithium ions through the electrolyte, and contributes to lowering of the coulombic efficiency of the battery. Concurrently, extensive dendrite growth can protrude through the separator, resulting in an internal short circuit; this ultimately can lead to thermal runaway and pose safety hazards for consumers. As such, researchers look towards improving the stability and uniformity of the SEI to mitigate the adverse effects on cyclability and safety in lithium anodes. Common approaches towards optimizing the SEI alter cell parameters by integrating scaffolds[77, 200, 183] and surface modifications via gaseous[13, 171, 196], chemical[113, 160, 158, 90], and physical[47, 84, 81, 23] treatments of the lithium electrode prior to battery operation. However, these approaches hinge on a strict control over reaction and ambient conditions. Similarly, electrolyte compositions are

altered via ion selective additives[106, 90, 7, 125] and report greater success in developing a controlled SEI that reduces side reactions with the electrolyte. These methods, however, involve a deliberate addition to the conventional cell parameters which adversely affect energy or power density and ultimately forgo scalability of lithium metal based batteries.

Recently, our group developed a versatile electrochemical approach towards the reinforcement of SEI layer in LiS batteries which evades the alteration of cell parameters[12]. Our approach optimizes standard cell operation protocols by simply accounting for the chemical reactions associated with specific voltage regions upon initial cycling, namely, the second discharge plateau (2.1 -1.7 V) associated with the reduction of short chain polysulfides and the formation of a solid film in LiS batteries[34, 177, 178]. Standard formation protocols simply operate a cell at a slow fixed rate within C/50-C/20 for a few cycles to allow for the formation of surface films[105, 52]. We found that by simply permitting more formation time (rate of C/100) during the second discharge plateau, LiS cells develop a noticeably more stable SEI[12]. Electrochemical characterization of LiS cells subject to the modified cell operation showed significant retention in capacity and coulombic efficiency which we attribute to the mitigation of polysulfide shuttling via a reinforced SEI in the carbon-sulfur cathode. This work seeks to extend the investigation to demonstrate the effects of controlled cell operation on dendrite suppression in lithium metal anodes for Li-S systems. Two-electrode symmetrical cells were utilized to isolate lithium metal anodes cycled within standard ether electrolyte (DOL: DME).

4.3   Methods

4.3.1   *Fabrication of Symmetrical Cells*

Symmetrical Li/Li cells were fabricated in 2032 type coin cells in an argon filled glove box. Bare lithium foils of 16 mm in diameter were used as both working and counter electrodes with Celgard 3501 separators. A conventional lithium-sulfur electrolyte was used for all cells (1:1 DOL:DME, 1wt% $LiNO_3$, 1M LiTFSI). All batteries were tested under room temperature with a Bio Logic VMP-3 for electrochemical procedures including galvanostatic cycling and potentiostatic electrochemical impedance spectroscopy (PEIS).

4.3.2   *Electrochemical Formation Procedure*

We investigated three electrochemical formation protocols for a duration of three complete discharge and charge cycles. To account for the difference in working-mechanisms in symmetrical cells versus cells with two distinct electrodes, cycling parameters were modeled after the amount of time LiS cells spent to complete a discharge/charge step at a given C rate.

The standard protocol, P1 models discharge rates of C/50 with a constant current of 168 μA, for the duration of time which sulfur cathodes completed the discharge/charge steps at that rate, 28 hours. Likewise, P2 models sulfur cells subject to a modified two-step discharge protocol (discharge C/50 for 2.8-2.1V, then C/100 for 2.1- 1.7 V) with discharge currents of 168 μA for 17 hrs, followed by 84 μA for 20 hrs. Charge steps for this protocol (C/50) are modeled by a current of 168 μA for 28 hrs. Finally, P3 subjects symmetrical cells to pulsed discharge and charge currents of 168 μA for 10-minute intervals, followed by

53

10-minute rests until LiS cells subject to the same procedure at C/50 reached full discharge or charge (125 repetitions per discharge and charge step).

Each formation protocol was followed by high rate cycling for 100 cycles. Wherein, LiS cells cycled at C/10 are modeled by symmetrical cells subject to a constant current of 6 mA for 1 hour durations for discharge and charge cycles.

4.3.3   *Electrochemical Cycling with PEIS Procedure*

The electrochemical formation procedures were repeated with PEIS employed after each discharge and charge cycle to further characterize the interfacial reactions occurring at this stage. P1 applied the following sequence for three repetitions before proceeding to cycling at a high C rate: rest, PEIS, 168 μA discharge, rest, PEIS, 168 μA charge, repeat two times. The following high rate cycling (C/10 for LiS half cells, 6 mA for symmetrical cells) employed PEIS every 10 cycles after the discharge and charge steps.

Similarly, P2 applied the following sequence for three repetitions before proceeding to cycling at a high C rate: rest, PEIS,168 μA + 84 μA discharge, rest, PEIS, 168 μA charge, repeat two times. The following high rate cycling employed PEIS every 10 cycles after the discharge and charge steps.

Lastly, P3 applied the following sequence for three repetitions before proceeding to cycling at a high C rate: rest, PEIS, 168 μA discharge for ten minutes, rest ten minutes, repeat 125 times, PEIS, 168 μA charge for 10 minutes, rest 10 minutes, repeat 125 times, repeat entire sequence three times.

4.3.4 *Characterization*

The morphology of lithium metal surfaces post cycling was characterized by a NovaNano Scanning Electron Microscope (NNS450) operated within 3-5 kV.

4.4 Results and Discussion

The symmetrical cell configuration is a practical tool for investigating interfacial chemistries on lithium metal anodes; the stability of potential profiles directly translates the stability of reactions between the lithium surface and the electrolyte. High rate cycling profiles for cells that have been subject to the different formation protocols are shown in Fig 4.1. Each profile shown is an average of three batteries subject to that particular formation protocol. Initial cycling for all protocols shows the largest overwork potential which is explained by the native surface film formed on lithium metal from the spontaneous electrolyte reduction. At this state, the film is expected to be the thickest and most homogeneous[15] which in effect noticeably hinders kinetics for lithium deposition and dissolution. Cells subject to the conventional formation protocol, P1, show an irregular evolution of overwork potential throughout the cycles. By cycle 20, overpotential of cells subject to P1 have decreased due to the improved local kinetics stemming from the cracks in native SEI which attract a nonuniform current distribution on the electrode, resulting in temporary decreased resistance. However, at cycle 30, overpotential rises again due to the rebuilding of the now irregular SEI, which slows down bulk kinetics of the cell since lithium deposition is accumulating on concentrated areas. This general trend repeats as the SEI developed during P1 is prone to cracking upon expansion because it was not formed uniformly enough during

the formation cycles. At cycle 50 for P1, we see a steady increased overpotential which can be attributed to an increased amount of dead lithium, surface dendrites observed in Fig 4.5d, that broke off during expansion of the SEI, and are now crowding the electrolyte. In contrast, P2 cells show stable voltage polarization throughout 100 cycles, despite the fast cycling current, suggesting that the two-step discharge formation currents enabled a more homogeneous surface film that effectively lowers the variability and density of local currents. However, the improved performance from P2 cannot directly be attributed to the partially reduced current rate compared to P1. A mere decrease in formation current does not guarantee improved performance; Fig S.1 shows an increased overpotential in cells that were subject to a consistent low current of 84 μA throughout the discharge cycles. This suggest that current rates are most impactful on the stability of interfacial chemistries during the end of a discharge cycle, as modeled by P2. Furthermore, the optimized local current density from P2 minimizes the extent of destructive lithium plating as observed by the decreased thickness of plated lithium compared to P1 (Fig 4.5c). Sparse dendrites formed on P2 cells Fig 4.5e are also supportive of a stable SEI which protected the lithium metal surface from excess side reactions.

P3 exhibits the narrowest overpotential within the initial cycles and between cycles 10-30, presuming to have the most stable interfacial chemistries among the tested formation protocols. However, the periodic voltage fluctuations observed are representative of local short-circuits which eventually result in global short circuit by cycle 88. A likely explanation for narrow overpotentials can be an increase in locally enhanced kinetics that stem from significant cracks in the SEI and plated lithium (Fig 4.5f) during the pulsed cycling. Similar

56
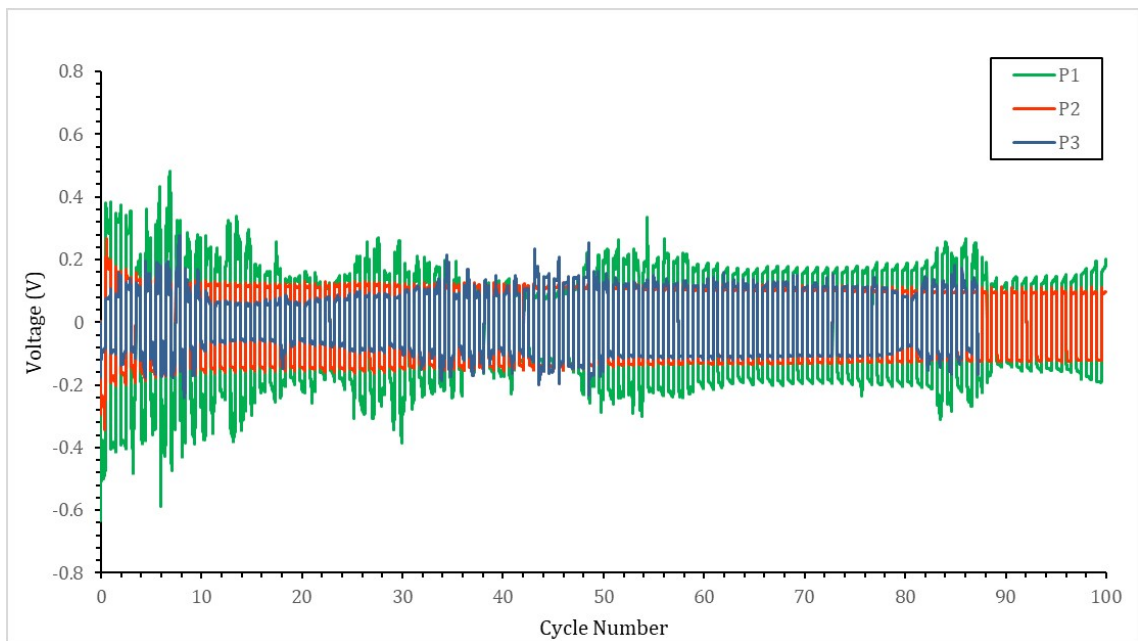
Figure 4.1: Evolution of overwork potentials for Li/Li symmetrical cells during high rate plating/stripping processes with current density of 3 mA cm^{-2}

to the pulsed cycling nature of P3, standard Galvanostatic Intermittent Titration Technique (GITT) profiles are shown to allow a cell's potential to rebound to a new equilibrium during the pulsed rest periods[146, 201]. This effectively causes strain upon frequent expansion and contraction within a given discharge/charge cycle. Significantly poor SEI in P3 cells is also supported by SEM images (Fig 4.5g) depicting dendrites order of magnitudes larger than dendrites found in P1 and P2. The large branch-like dendrites were able to grow more freely because less of the lithium metal surface was protected by a native SEI; in other words, fresh lithium metal was constantly reducing electrolyte and forming larger dendrites.

Potentiostatic Electrochemical Impedance Spectroscopy (PEIS) was employed during the different formation protocols to further investigate the kinetics, thermodynamic properties and diffusion behaviors inside the electrolyte bulk and at the interfaces of sym-
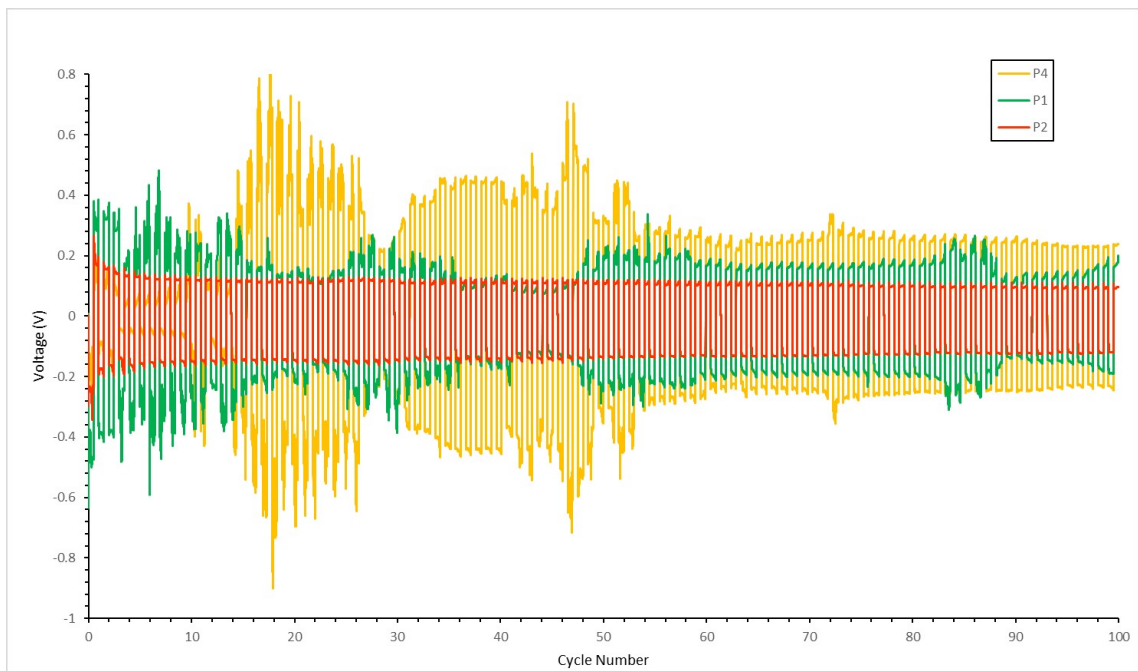
Figure 4.2: Evolution of overwork potentials for Li/Li symmetrical cells during high rate plating/stripping processes with current density of 3 mA cm^{-2}

metrical cells. In this study, a voltage signal of 10 mV was used within a frequency range 10 kHz - 10 mHz. Impedance data was acquired at the end of each discharge and charge sequence for the three formation cycles within each protocol. As shown in Nyquist Plots of PEIS, Fig 4.3, the diameter of semicircles indicate the charge transfer resistance (Rct) at the double layers. Although both electrodes of the symmetric cells are lithium metal, they can never be chemically/electrochemically identical. In order to distinguish, terms discharge and charge are maintained in this study. Fig 4.3(a-c) isolate Nyquist plots for discharge cycles to highlight the effects of formation discharge rates on lithium metal anodes. Similarly, Fig 4.3(d-f) depict Nyquist plots for the formation charge cycles for protocols P1-P3. The decreasing impedance value in all figures are attributed to the gradual transition from local to bulk reactions, considering that the initial formation cycles depict prelimi-

nary wetting and development of native surface films. All protocols, with the exception of P3, have similar starting impedance due to the inert oxidized surface of lithium foils. P3 shows exceptionally higher Rct during the 1st discharge, suggesting that the pulsed cycling style is destructive upon initial discharging. By the third discharge cycles, P2 cells show a 4-fold decrease in Rct compared to that of the conventional P1 cells. This suggests that the discharge rates during formation benefit the surface area of surface films. Besides, all semicircles for P2 exhibit pronounced diffusion tails relative to the other formation protocols, which is evidence for the formation of beneficial surface area[32] for fast lithium-ion diffusion. It can be attributed to the more favorable morphology of the SEI layers forming at the interfaces. The formation of this structure reduces the possibility of the lithium ions to participate into plating and other parasitic reactions. Instead, most of the lithium ions diffuse and intercalate in the formed structure which dramatically decreases the impedance of the cell.

Figure 4.3: Nyquist plots measured after formation charge cycles for cells subject to (A) P1, (B) P2, (C) P3; and after formation discharge cycles for (D) P1, (E) P2, (F) P3.

To further characterize the interfacial variations occurring in the cells during formation protocols, Bode plots of the same PEIS results are shown in Fig 4.4. Compared with Nyquist plot, Bode plots provide a detailed insight into the phase changes along the frequency spectrum, wherein, the phase changes from high to low frequency are depicted as valleys in Bode figures. Valleys that undergo significant changes in depth are indicative of inconsistent reactions occurring at the electrode surface. The drastic depth change from -20°to -5 for P2 cells (Fig 4.4 b, e) is therefore telling of unique reactions occurring within the formation protocol that are not present in P1 formation. Inconsistent reaction during these formation cycles can be representative of SEI formation since that process is expected to be more heterogeneous than plating in Li-Li symmetrical cells. Thus, we can infer the drastic depth change in the Bode valleys for P2 represent formation of robust SEI in comparison to P1, which is supportive of the stable high rate cycling of P2 in Fig 4.1. Cells

that have minimal SEI layer are more prone to homogeneous lithium plating, and thus experience less diffusion behavior than cells with anomalous morphology due to a developed SEI layer. Furthermore, the phase angle change observed at the lower frequency range for P2 cells indicates the existence of the nanostructure which has a semi-infinite diffusion length. Such behavior cannot be observed for P1 due to the lack of diffusion behavior for the lithium surfaces that are more prone to plating. The significant phase change during the discharge cycles of P3 cannot be explained by the same phenomena as P2, as it is a result of the abnormally high initial impedance. After stabilization, P3 experiences minimal phase change comparable to P1.

Therefore, it is evident that for P2, the morphology of the SEI layers is beneficial for the rapid ionic diffusion and thus avoids metallic dendrite formation. Besides, the cycling data in Fig 4.1 further supports the analysis given above. For protocols P1 and P3, various voltage fluctuations can be observed, which indicates complicated reactions happening at the interfaces, including dendrite formation and SEI dissolution. All these reactions lead to the poor polarization behavior. However, due to the favorable morphology and possibly nanostructured lithium surface of P2, the cycling behavior is very stable.
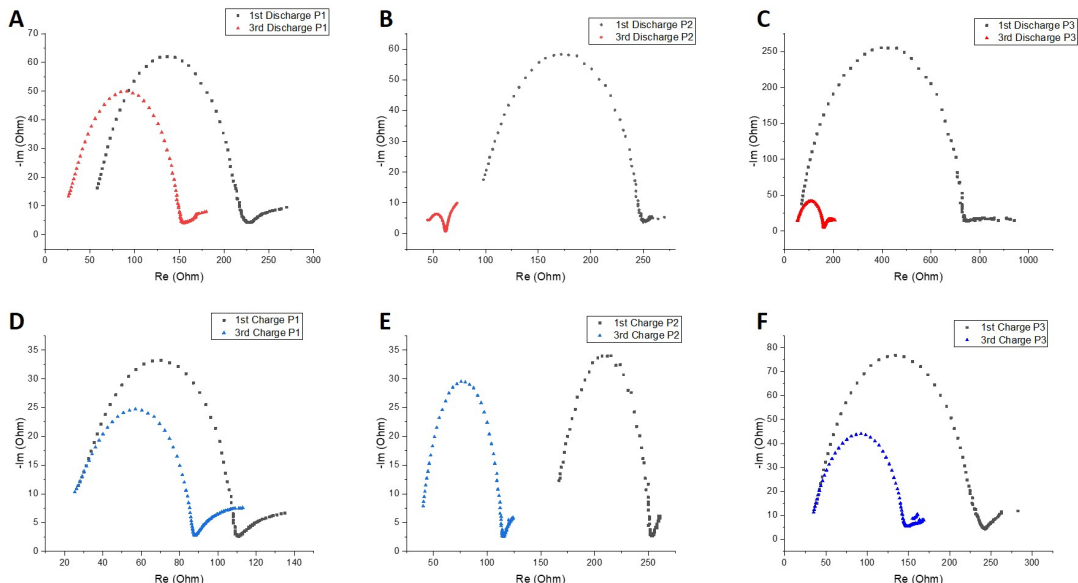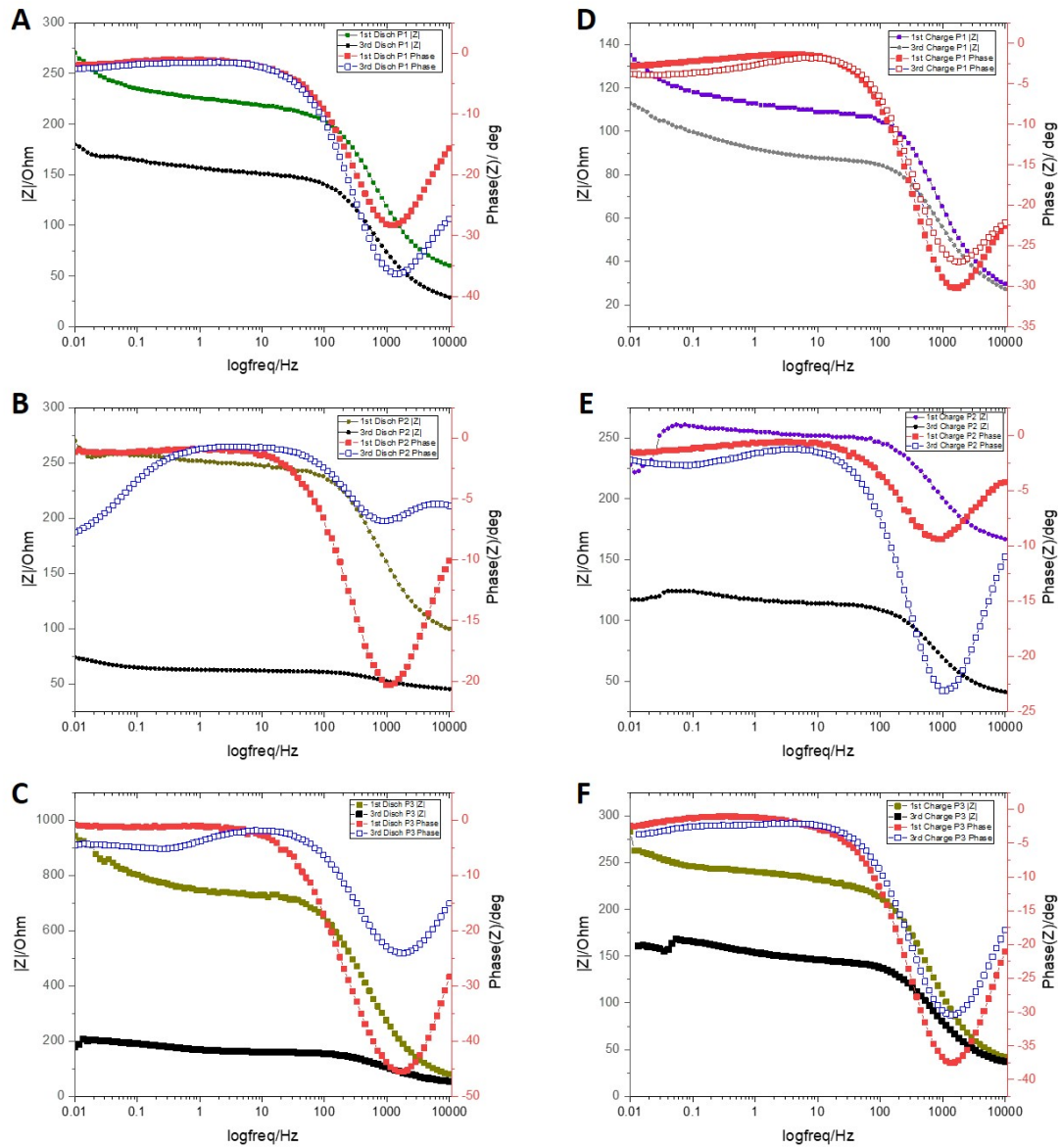
Figure 4.4: Bode measurements taken after formation charge cycles for cells subject to (A) P1, (B) P2, (C) P3; and after formation discharge cycles for (D) P1, (E) P2, (F) P3.

Symmetrical cells are inevitably prone to lithium plating on both electrodes, as illustrated by Fig 4.5a, and are at higher risk than conventional cells to experience an accumulation of detached plated lithium in the separator thereby, leaving a cell at hazard of a short circuit. However, an analysis on the effect of formation protocols on plating in symmetrical cells can guide safe cell operation in full cells incorporating lithium metal. Wherein, the extent of plating in response to formation protocols can provide further insights towards the stability of interfacial chemistries within the cells. The morphology of surface films containing plated lithium and dendrites was characterized post cycling with Scanning Electron Microscopy (SEM). The widths of plated lithium highlighted yellow in Fig 4.5b,c were obtained using ImageJ processing; the width of plated lithium decreased to 190 μm when cells were subject to P2, in comparison to the 284 μm plated film for cells subject to P1. The notable reduction of plated lithium corresponds to an improved balance between the rate of lithium intercalation and lithium deposition for cells that were activated by P2. Whereas the increased plating for P1 further explain the overpotential spikes in Fig 4.1.

Furthermore, SEM images taken at the lithium surfaces show a drastic change in the popularity and size of dendrites for each formation protocol. Images for P1 cells depict dendrites as small white limbs, dispersed evenly throughout the electrode (Fig 4.5d). In contrast, dendrites are found in areas of sparse population for lithium surfaces subject to P2 (Fig 4.5e). The surface film morphology of P3 cells differ significantly to that observed for P1 and P2 cells. Interestingly, the pulsed nature of this protocol prevented uniform lithium plating, inferring a mechanically unstable SEI layer that cannot withstand frequent volume fluctuations, thus enabling the large mosaic-like cracks visible in Fig 4.5f which act as kinetic
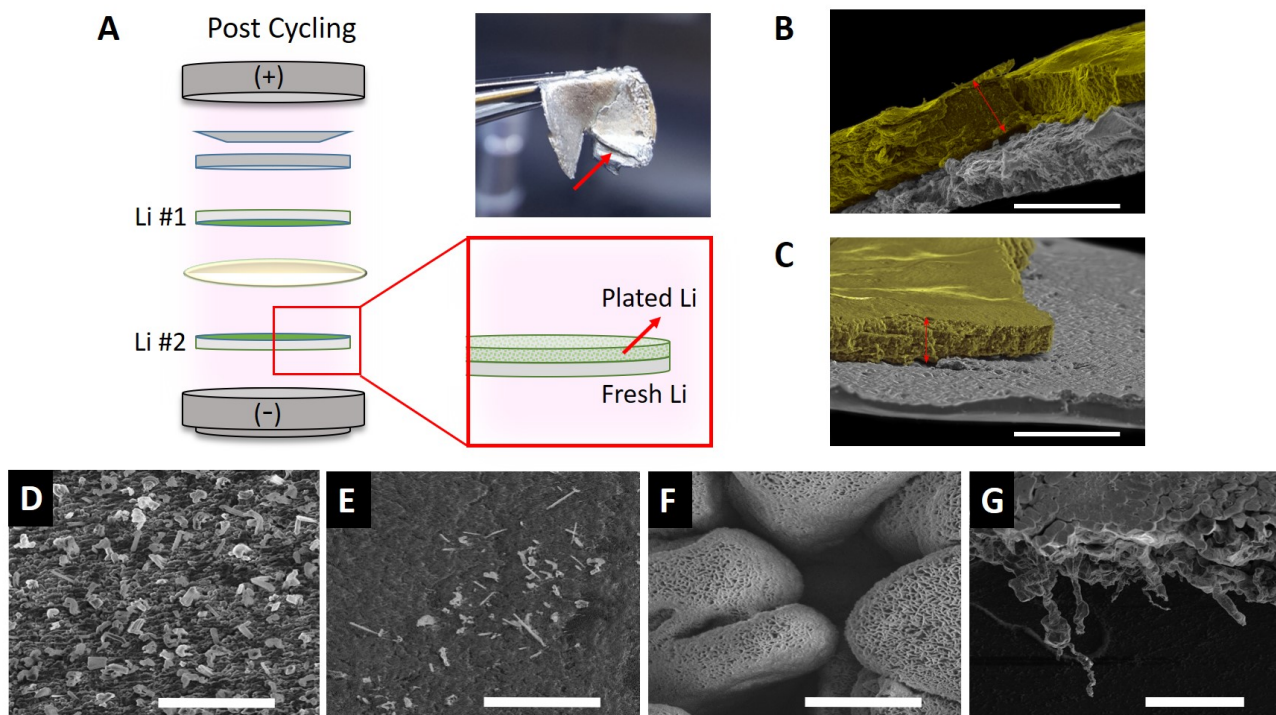
Figure 4.5: Illustrations of plated Li as (A) a schematic, and as cross-sectional SEM images highlighted in yellow with 500 μm scale for (B) P1 cells, and (C) P2 cells. Surface SEM images of plated Li with 10 μm scale for (D) P1 cells, (E) P2 cells, (F) P3 cells; and 100 μm scale for (G) P3 cells.

pathways for lithium deposition[93]. Additionally, the surfaces of the mosaic structures are covered with nano moss-like lithium which are considered to be reaction limited[3]; the intermittent cycling style of P3 is likely to have influenced the reaction rates to form mossy lithium. Studies on Li-Li symmetrical cells have observed that once mossy lithium depletes electrolyte salt on the anode surface, it ignites sudden growth of branch-like dendrites and is observed by a voltage spike as seen in Fig 4.1 around 34 cycles for P3. Mossy lithium and branch-like dendrites found in Fig 4.5g are likely to have caused the cell failures for P3 as observed in Fig 4.1, either due to electrolyte depletion or cell shortage via piercing of the separator.

4.5 Highlights

Lithium metal is a promising anode for lithium ion batteries, especially in the lithium-sulfur architecture. However, both electrodes have their individual challenges which hinder their commercialization; polysulfide shuttling, dendrite formation and unstable SEI layers lead to more complex cycling mechanisms than conventional transition metal oxide/graphite batteries. Consequently, conventional cell operation and electrochemical characterization techniques need to be adapted for the new generation of lithium batteries. This paper showcases a practical approach for controlling dendrite formation, and SEI morphology and stability in lithium metal anodes via tailored formation protocols. Symmetrical cells subject to the tailored discharge rates displayed advantages in steadily enduring high cycling currents of 6 mA with minimal polarization, and in lowering the charge transfer resistance at the cell interfaces. Moreover, this approach yields smooth surface morphology

65

of lithium anodes which minimize lithium plating and significantly suppress nucleation sites for dendrite growth.

These findings highlight the impact of deliberate formation protocols on surface chemistries for a given material system. By fully exploiting cell operation in parallel to optimizing cell parameters for individual electrode chemistries, stable next generation full cell systems such as LiS can be achieved. Further developments on this approach are contingent on a thorough analysis of formation current rates for LiS batteries that can conserve practical cycling time. It is possible that conventional formation rates of C/5-C/20 are too demanding and can cause micro-localized short circuits given the inert nature of sulfur cathodes. Although a combination of slow current rates of C/50-C/100 presented here prove to be effective, it would be beneficial to explore current rates governed by areal capacity to promote homogeneous activation of electrodes.

Chapter 5

Conclusions

The primary objective of this dissertation is to present sustainable technologies that can contribute to mitigating the environmental impacts of fossil fuel industries. Chapter 2 highlights a novel sponge material for oil recovery in marine spills. Despite the sponge's effectiveness at separating oil from water, improvements can be made on the structure's elasticity to broaden its sorption applications. Furthermore, modifications can be made on the sponge's crystallinity to improve its candidacy as a conductive host for lithium ion electrodes. This can be achieved by exchanging the iron metal catalysts in the sponge synthesis process to a metal which would not react unfavorably with sulfur. For example, the use of silver nitrate as a catalyst would eliminate the need for extensive etching treatments which disrupt the graphitic properties of the sponge. Hence, the resulting structure would maintain higher crystallinity than that of the Fe-based sponge presented here for sponge-sulfur cathodes.

The following chapters, 3 and 4, deviate from conventional materials-research for Li-S batteries to address areas of research which have not garnered enough attention, yet have equal impact a cell's electrochemistry. Chapter 3 covers scalable production methods such as large scale optimization of slurry densities on sulfur and silicon electrodes which are later used in the redesign of full cell architectures. Cell operation investigations are covered in Chapter 3 for sulfur cathodes, and in Chapter 4 for lithium metal anodes. In the case for sulfur cathodes, reinforced solid electrolyte interfaces retain cell capacity by minimizing excess solubility of long chain polysulfides in the electrolyte. In a like manner, the solid electrolyte interface on lithium anodes improved cycling stability by suppressing growth of dendritic and plated lithium.

The applied-research techniques presented herein were employed on base electrodes composed of standard, commercially available materials merely to isolate the impact of the methodology. Nonetheless, it is recommended to use applied-research techniques in parallel to materials-research to obtain the best performance and fundamental understanding of electrochemistry in next-generation batteries. Although the applied-research methods presented here are tailored for lithium-sulfur batteries, they can be modified to fit any of the up-and-coming lithium battery systems such as solid state, and lithium air batteries.

Finally, given that lithium ion batteries have become widely adopted in interest to mitigate environmental impacts from fossil energy, the new industry has to be mindful of sustainable production practices. This includes safe mining of materials including lithium and other active materials, as well as safe disposal of battery waste to prevent catastrophic environmental impacts as we are seeing for the fossil energy industry.

Bibliography

[1] 14 2. GLOBAL WIND STATISTICS 2017.

[2] Francisco M Baena-Moreno, Mónica Rodríguez-Galán, Fernando Vega, Bernabé Alonso-Fariñas, Luis F Vilches Arenas, and Benito Navarrete. Carbon capture and utilization technologies: a literature review and recent advances. *Energy Sources Part A*, pages 1–31, November 2018.

[3] Peng Bai, Ju Li, Fikile R Brushett, and Martin Z Bazant. Transition of lithium growth mechanisms in liquid electrolytes. *Energy Environ. Sci.*, 9(10):3221–3229, 2016.

[4] Juan Balach, Tony Jaumann, Markus Klose, Steffen Oswald, Jürgen Eckert, and Lars Giebeler. Functional mesoporous Carbon-Coated separator for Long-Life, High-Energy Lithium–Sulfur batteries. *Adv. Funct. Mater.*, 25(33):5285–5291, 2015.

[5] Anthony Barré, Benjamin Deguilhem, Sébastien Grolleau, Mathias Gérard, Frédéric Suard, and Delphine Riu. A review on lithium-ion battery ageing mechanisms and estimations for automotive applications. *J. Power Sources*, 241:680–689, November 2013.

[6] Elliott P Barrett, Leslie G Joyner, and Paul P Halenda. The determination of pore volume and area distributions in porous substances. i. computations from nitrogen isotherms, 1951.

[7] A Basile, A I Bhatt, and A P O'Mullane. Stabilizing lithium metal using ionic liquids for long-lived batteries. *Nat. Commun.*, 7:ncomms11794, June 2016.

[8] I Bauer, S Thieme, J Brückner, H Althues, and S Kaskel. Reduced polysulfide shuttle in lithium–sulfur batteries using nafion-based separators, 2014.

[9] Hamed Hosseini Bay, Daisy Patino, Zafer Mutlu, Paige Romero, Mihrimah Ozkan, and Cengiz S Ozkan. Scalable multifunctional ultra-thin graphite sponge: Free-standing, superporous, superhydrophobic, oleophilic architecture with ferromagnetic properties for environmental cleaning. *Sci. Rep.*, 6:21858, February 2016.

[10] A Beitollahi, H Hosseini-Bay, and H Sarpoolaki. Synthesis and characterization of Al2O3–ZrO2 nanocomposite powder by sucrose process, 2010.

[11] Jeffrey Bell, Rachel Ye, Kazi Ahmed, Chueh Liu, Mihrimah Ozkan, and Cengiz S Ozkan. Free-standing Ni–NiO nanofiber cloth anode for high capacity and high rate li-ion batteries. *Nano Energy*, 18:47–56, November 2015.

[12] Jeffrey Bell, Rachel Ye, Daisy Patino, Kazi Ahmed, Andrew Scott, Leon Peng, Zafer Mutlu, Mihrimah Ozkan, and Cengiz S Ozkan. Plateau targeted conditioning: An additive-free approach towards robust SEI formation in Li-S batteries for enhanced capacity and cycle life. *Nano Energy*, 49:498–507, July 2018.

[13] D G Belov, O V Yarmolenko, A Peng, and O N Efimov. Lithium surface protection by polyacetylene in situ polymerization. *Synth. Met.*, 156(9):745–751, May 2006.

[14] Hengchang Bi, Zongyou Yin, Xiehong Cao, Xiao Xie, Chaoliang Tan, Xiao Huang, Bo Chen, Fangtao Chen, Qingling Yang, Xinyang Bu, Xuehong Lu, Litao Sun, and Hua Zhang. Carbon fiber aerogel made from raw cotton: a novel, efficient and recyclable sorbent for oils and organic solvents. *Adv. Mater.*, 25(41):5916–5921, November 2013.

[15] Georg Bieker, Martin Winter, and Peter Bieker. Electrochemical in situ investigations of SEI and dendrite formation on the lithium metal anode. *Phys. Chem. Chem. Phys.*, 17(14):8670–8679, April 2015.

[16] I A Buist, S G Potter, B K Trudel, S R Shelnutt, Ann Hayward Walker, D K Scholz, Per Johan Brandvik, Janne Fritt-Rasmussen, A A Allen, and Paul Smith. In situ burning in ice-affected waters: state of knowledge report. *Final report*, 7(1), 2013.

[17] Martin Rolf Busche, Philipp Adelhelm, Heino Sommer, Holger Schneider, Klaus Leitner, and Jürgen Janek. Systematical electrochemical study on the parasitic shuttle-effect in lithium-sulfur-cells at different temperatures and different rates. *J. Power Sources*, 259:289–299, August 2014.

[18] Jinjun Cai, Menglong Yang, Yanlong Xing, and Xuebo Zhao. Large surface area sucrose-based carbons via template-assisted routes: Preparation, microstructure, and hydrogen adsorption properties. *Colloids Surf. A Physicochem. Eng. Asp.*, 444:240–245, March 2014.

[19] Kunpeng Cai, Min-Kyu Song, Elton J Cairns, and Yuegang Zhang. Nanostructured Li2S–C composites as cathode material for High-Energy Lithium/Sulfur batteries. *Nano Lett.*, 12(12):6474–6479, December 2012.

[20] Paola Calcagnile, Despina Fragouli, Ilker S Bayer, George C Anyfantis, Luigi Martiradonna, P Davide Cozzoli, Roberto Cingolani, and Athanassia Athanassiou. Magnetically driven floating foams for the removal of oil contaminants from water. *ACS Nano*, 6(6):5413–5419, June 2012.

[21] Natalia A Cañas, Kei Hirose, Brigitta Pascucci, Norbert Wagner, K Andreas Friedrich, and Renate Hiesgen. Investigations of lithium–sulfur batteries using electrochemical impedance spectroscopy. *Electrochim. Acta*, 97:42–51, May 2013.

[22] Ruiguo Cao, Wu Xu, Dongping Lv, Jie Xiao, and Ji-Guang Zhang. Anodes for rechargeable Lithium-Sulfur batteries. *Advanced Energy Materials*, 5(16):1402273, 2015.

[23] Yanqiang Cao, Xiangbo Meng, and Jeffrey W Elam. Atomic layer deposition of li x al y S Solid-State electrolytes for stabilizing Lithium-Metal anodes. *ChemElectroChem*, 3(6):858–863, June 2016.

[24] Claire L Carlson and Domy C Adriano. Environmental impacts of coal combustion residues. *J. Environ. Qual.*, 22:227–247, 1993.

[25] Victor Chabot, Drew Higgins, Aiping Yu, Xingcheng Xiao, Zhongwei Chen, and Jiujun Zhang. A review of graphene and graphene oxide sponge: material synthesis and applications to energy and the environment. *Energy Environ. Sci.*, 7(5):1564–1596, 2014.

[26] Candace K Chan, Riccardo Ruffo, Seung Sae Hong, and Yi Cui. Surface chemistry and morphology of the solid electrolyte interphase on silicon nanowire lithium-ion battery anodes. *J. Power Sources*, 189(2):1132–1140, April 2009.

[27] Duck-Rye Chang, Suck-Hyun Lee, Sun-Wook Kim, and Hee-Tak Kim. Binary electrolyte based on tetra(ethylene glycol) dimethyl ether and 1,3-dioxolane for lithium–sulfur battery, 2002.

[28] Haiqun Chen, Marc B Müller, Kerry J Gilmore, Gordon G Wallace, and Dan Li. Mechanically strong, electrically conductive, and biocompatible graphene paper, 2008.

[29] Jia-Jia Chen, Ru-Ming Yuan, Jia-Min Feng, Qian Zhang, Jing-Xin Huang, Gang Fu, Ming-Sen Zheng, Bin Ren, and Quan-Feng Dong. Conductive lewis base matrix to recover the missing link of Li2S8 during the sulfur redox cycle in Li–S battery, 2015.

[30] Shu-Ru Chen, Yun-Pu Zhai, Gui-Liang Xu, Yan-Xia Jiang, Dong-Yuan Zhao, Jun-Tao Li, Ling Huang, and Shi-Gang Sun. Ordered mesoporous carbon/sulfur nanocomposite of high performances as cathode for lithium–sulfur battery, 2011.

[31] Zongping Chen, Chuan Xu, Chaoqun Ma, Wencai Ren, and Hui-Ming Cheng. Lightweight and flexible graphene foam composites for high-performance electromagnetic interference shielding. *Adv. Mater.*, 25(9):1296–1300, 2013.

[32] Xin-Bing Cheng, Hong-Jie Peng, Jia-Qi Huang, Fei Wei, and Qiang Zhang. Dendrite-free nanostructured anode: entrapment of lithium in a 3D fibrous matrix for ultra-stable lithium-sulfur batteries. *Small*, 10(21):4257–4263, November 2014.

[33] Sang-Eun Cheon, Ki-Seok Ko, Ji-Hoon Cho, Sun-Wook Kim, Eog-Yong Chin, and Hee-Tak Kim. Rechargeable lithium sulfur battery, 2003.

[34] Sang-Eun Cheon, Ki-Seok Ko, Ji-Hoon Cho, Sun-Wook Kim, Eog-Yong Chin, and Hee-Tak Kim. Rechargeable lithium sulfur battery: I. structural change of sulfur cathode during discharge and charge. *J. Electrochem. Soc.*, 150(6):A796–A799, June 2003.

[35] Joon Hyung Cho and So Young Sohn. A novel decomposition analysis of green patent applications for the evaluation of R&D efforts to reduce CO2 emissions from fossil fuel energy consumption. `https://www.sciencedirect.com/science/article/pii/S0959652618313908/pdfft?md5=486f792d4738418465e8456cd2815792&pid=1-s2.0-S0959652618313908-main.pdf&isDTMRedir=true&download=true`. Accessed: 2019-1-18.

[36] N S Choi, Z Chen, S A Freunberger, X Ji, and others. Challenges facing lithium batteries and electrical doublelayer capacitors. *Angew. Chem. Int. Ed Engl.*, 2012.

[37] Ying Chu and Qinmin Pan. Three-dimensionally macroporous Fe/C nanocomposites as highly selective oil-absorption materials. *ACS Appl. Mater. Interfaces*, 4(5):2420–2425, May 2012.

[38] T Cleaver, P Kovacik, M Marinescu, T Zhang, and others. Perspective—Commercializing lithium sulfur batteries: Are we doing the right research? *Journal of The*, 2018.

[39] R N Das. Nanocrystalline ceramics from sucrose process, 2001.

[40] Dennis W Dees, Shigehiro Kawauchi, Daniel P Abraham, and Jai Prakash. Analysis of the galvanostatic intermittent titration technique (GITT) as applied to a lithium-ion porous electrode. *J. Power Sources*, 189(1):263–268, April 2009.

[41] Nathalie Delpuech, Nicolas Dupre, Philippe Moreau, Jean-Sebastian Bridel, Joel Gaubicher, Bernard Lestriez, and Dominique Guyomard. Mechanism of silicon electrode aging upon cycling in full Lithium-Ion batteries, 2016.

[42] Zhaofeng Deng, Zhian Zhang, Yanqing Lai, Jin Liu, Jie Li, and Yexiang Liu. Electrochemical impedance spectroscopy study of a Lithium/Sulfur battery: Modeling and analysis of capacity fading. *J. Electrochem. Soc.*, 160(4):A553–A558, January 2013.

[43] Ning Ding, Lan Zhou, Changwei Zhou, Dongsheng Geng, Jin Yang, Sheau Wei Chien, Zhaolin Liu, Man-Fai Ng, Aishui Yu, T S Andy Hor, Michael B Sullivan, and Yun Zong. Building better lithium-sulfur batteries: from LiNO3 to solid oxide catalyst. *Sci. Rep.*, 6:33154, September 2016.

[44] Xiaochen Dong, Jun Chen, Yanwen Ma, Jing Wang, Mary B Chan-Park, Xiangmei Liu, Lianhui Wang, Wei Huang, and Peng Chen. Superhydrophobic and superoleophilic hybrid foam of graphene and carbon nanotube for selective removal of oils or organic solvents from the surface of water. *Chem. Commun.*, 48(86):10660–10662, 2012.

[45] Ya-Lei Dong, Hui-Ge Zhang, Zia Ur Rahman, Li Su, Xiao-Jiao Chen, Jing Hu, and Xing-Guo Chen. Graphene oxide-Fe3O4 magnetic nanocomposites with peroxidase-like activity for colorimetric detection of glucose. *Nanoscale*, 4(13):3969–3976, July 2012.

[46] Gang Du, Chuanwang Sun, Xiaoling Ouyang, and Chi Zhang. A decomposition analysis of energy-related CO2 emissions in chinese six high-energy intensive industries. *J. Clean. Prod.*, 184:1102–1112, May 2018.

[47] Nancy J Dudney. Addition of a thin-film inorganic solid electrolyte (lipon) as a protective film in lithium batteries with a liquid electrolyte. *J. Power Sources*, 89(2):176–179, August 2000.

[48] Omar Ellabban, Haitham Abu-Rub, and Frede Blaabjerg. Renewable energy resources: Current status, future prospects and their enabling technology. *Renewable Sustainable Energy Rev.*, 39:748–764, November 2014.

[49] Zhuang-Jun Fan, Wang Kai, Jun Yan, Tong Wei, Lin-Jie Zhi, Jing Feng, Yue-Ming Ren, Li-Ping Song, and Fei Wei. Facile synthesis of graphene nanosheets via fe reduction of exfoliated graphite oxide. *ACS Nano*, 5(1):191–198, January 2011.

[50] Zhuangjun Fan, Jun Yan, Linjie Zhi, Qiang Zhang, Tong Wei, Jing Feng, Milin Zhang, Weizhong Qian, and Fei Wei. A three-dimensional carbon nanotube/graphene sandwich and its application as electrode in supercapacitors. *Adv. Mater.*, 22(33):3723–3728, 2010.

[51] Zachary Favors, Wei Wang, Hamed Hosseini Bay, Aaron George, Mihrimah Ozkan, and Cengiz S Ozkan. Stable cycling of SiO2 nanotubes as High-Performance anodes for Lithium-Ion batteries, 2015.

[52] Zachary Favors, Wei Wang, Hamed Hosseini Bay, Zafer Mutlu, Kazi Ahmed, Chueh Liu, Mihrimah Ozkan, and Cengiz S Ozkan. Scalable synthesis of nano-silicon from beach sand for long cycle life li-ion batteries. *Sci. Rep.*, 4:5623, July 2014.

[53] Lin Feng, Zhongyi Zhang, Zhenhong Mai, Yongmei Ma, Biqian Liu, Lei Jiang, and Daoben Zhu. A Super-Hydrophobic and Super-Oleophilic coating mesh film for the separation of oil and water, 2004.

[54] X J Feng and L Jiang. Design and creation of Superwetting/Antiwetting surfaces. *Adv. Mater.*, 18(23):3063–3078, December 2006.

[55] Y Fernández Fernández, M A Fernández López, and B Olmedillas Blanco. Innovation for sustainability: The impact of R&D spending on CO2 emissions. *J. Clean. Prod.*, 172:3459–3467, January 2018.

[56] A C Ferrari, J C Meyer, V Scardaci, C Casiraghi, M Lazzeri, F Mauri, S Piscanec, D Jiang, K S Novoselov, S Roth, and A K Geim. Raman spectrum of graphene and graphene layers. *Phys. Rev. Lett.*, 97(18):187401, November 2006.

[57] Andrea C Ferrari. Raman spectroscopy of graphene and graphite: Disorder, electron–phonon coupling, doping and nonadiabatic effects. *Solid State Commun.*, 143(1):47–57, July 2007.

[58] Andrea C Ferrari and Denis M Basko. Raman spectroscopy as a versatile tool for studying the properties of graphene. *Nat. Nanotechnol.*, 8(4):235–246, April 2013.

[59] Mervin Fingas. *Oil Spill Science and Technology.* Gulf Professional Publishing, November 2016.

[60] L Gagneur, A L Driemeyer-Franco, C Forgez, and G Friedrich. Modeling of the diffusion phenomenon in a lithium-ion cell using frequency or time domain identification. *Microelectron. Reliab.*, 53(6):784–796, June 2013.

[61] Xuchun Gui, Hongbian Li, Kunlin Wang, Jinquan Wei, Yi Jia, Zhen Li, Lili Fan, Anyuan Cao, Hongwei Zhu, and Dehai Wu. Recyclable carbon nanotube sponges for oil absorption. *Acta Mater.*, 59(12):4798–4804, July 2011.

[62] Xuchun Gui, Jinquan Wei, Kunlin Wang, Anyuan Cao, Hongwei Zhu, Yi Jia, Qinke Shu, and Dehai Wu. Carbon nanotube sponges. *Adv. Mater.*, 22(5):617–621, February 2010.

[63] Juchen Guo, Yunhua Xu, and Chunsheng Wang. Sulfur-Impregnated disordered carbon nanotubes cathode for Lithium–Sulfur batteries. *Nano Lett.*, 11(10):4288–4294, October 2011.

[64] Jusef Hassoun, Junghoon Kim, Dong-Ju Lee, Hun-Gi Jung, Sung-Man Lee, Yang-Kook Sun, and Bruno Scrosati. A contribution to the progress of high energy batteries: A metal-free, lithium-ion, silicon–sulfur battery. *J. Power Sources*, 202:308–313, March 2012.

[65] Yu He, Xiqian Yu, Yanhong Wang, Hong Li, and Xuejie Huang. Alumina-coated patterned amorphous silicon as the anode for a lithium-ion battery with high coulombic efficiency. *Adv. Mater.*, 23(42):4938–4941, 2011.

[66] Shuo Huang, Yuhong Jin, and Mengqiu Jia. Preparation of graphene/Co3O4 composites by hydrothermal method and their electrochemical properties. *Electrochim. Acta*, 95:139–145, April 2013.

[67] Dale?l Huber. Synthesis, properties, and applications of iron nanoparticles, 2005.

[68] Md Mahbubul Islam, Alireza Ostadhossein, Oleg Borodin, A Todd Yeates, William W Tipton, Richard G Hennig, Nitin Kumar, and Adri C T van Duin. ReaxFF molecular dynamics simulations on lithiated sulfur cathode materials, 2015.

[69] Irena B Ivshina, Maria S Kuyukina, Anastasiya V Krivoruchko, Andrey A Elkin, Sergey O Makarov, Colin J Cunningham, Tatyana A Peshkur, Ronald M Atlas, and James C Philp. Oil spill problems and sustainable response strategies through new technologies. *Environ. Sci. Process. Impacts*, 17(7):1201–1219, July 2015.

[70] Mark Jaccard. *Sustainable Fossil Fuels: The Unusual Suspect in the Quest for Clean and Enduring Energy.* Cambridge University Press, January 2006.

[71] Liwen Ji, Mumin Rao, Shaul Aloni, Lei Wang, Elton J Cairns, and Yuegang Zhang. Porous carbon nanofiber–sulfur composite electrodes for lithium/sulfur cells. *Energy Environ. Sci.*, 4(12):5053–5059, November 2011.

[72] Xiulei Ji, Kyu Tae Lee, and Linda F Nazar. A highly ordered nanostructured carbon–sulphur cathode for lithium–sulphur batteries. *Nat. Mater.*, 8:500, May 2009.

[73] Seung Won Jung, Oh Youn Kwon, Chang Kyu Joo, Jung-Hoon Kang, Moonkoo Kim, Won Joon Shim, and Young-Ok Kim. Stronger impact of dispersant plus crude oil on natural plankton assemblages in short-term marine mesocosms. *J. Hazard. Mater.*, 217-218:338–349, May 2012.

[74] Katharina Karner, Russell McKenna, Marian Klobasa, and Thomas Kienberger. Industrial excess heat recovery in industry-city networks: a technical, environmental and economic assessment of heat flexibility. *J. Clean. Prod.*, 193:771–783, August 2018.

[75] K Christian Kemp, Humaira Seema, Muhammad Saleh, Nhien H Le, Kandula Mahesh, Vimlesh Chandra, and Kwang S Kim. Environmental applications using graphene composites: water remediation and gas adsorption. *Nanoscale*, 5(8):3149–3171, April 2013.

[76] Hyunjung Kim, Byunghee Han, Jaebum Choo, and Jaephil Cho. Three-dimensional porous silicon particles for use in high-performance lithium secondary batteries. *Angew. Chem. Int. Ed Engl.*, 120(52):10305–10308, 2008.

[77] Joo-Seong Kim, Dae Woo Kim, Hee Tae Jung, and Jang Wook Choi. Controlled lithium dendrite growth by a synergistic effect of multilayered graphene coating and an electrolyte additive. *Chem. Mater.*, 27(8):2780–2787, April 2015.

[78] Katharina Kohse-Höinghaus. Clean combustion: Chemistry and diagnostics for a systems approach in transportation and energy conversion. *Prog. Energy Combust. Sci.*, 65:1–5, March 2018.

[79] Weihe Kong, Hong Li, Xuejie Huang, and Liquan Chen. Gas evolution behaviors for several cathode materials in lithium-ion batteries. *J. Power Sources*, 142(1):285–291, March 2005.

[80] Richa Kothari, V V Tyagi, and Ashish Pathak. Waste-to-energy: A way from renewable energy sources to sustainable development. *Renewable Sustainable Energy Rev.*, 14(9):3164–3170, December 2010.

[81] Alexander C Kozen, Chuan-Fu Lin, Alexander J Pearse, Marshall A Schroeder, Xiaogang Han, Liangbing Hu, Sang-Bok Lee, Gary W Rubloff, and Malachi Noked. Next-Generation lithium metal anode engineering via atomic layer deposition. *ACS Nano*, 9(6):5884–5892, June 2015.

[82] Deuk Sin Kwon, Joon Hyung Cho, and So Young Sohn. Comparison of technology efficiency for CO2 emissions reduction among european countries based on DEA with decomposed factors. *J. Clean. Prod.*, 151:109–120, May 2017.

[83] Jialiang Lang, Longhao Qi, Yuzi Luo, and Hui Wu. High performance lithium metal anode: Progress and prospects. *Energy Storage Materials*, 7:115–129, April 2017.

[84] Hongkyung Lee, Dong Jin Lee, Yun-Jung Kim, Jung-Ki Park, and Hee-Tak Kim. A simple composite protective layer coating that enhances the cycling stability of lithium metal batteries. *J. Power Sources*, 284:103–108, June 2015.

[85] Jeong Woo Lee, Jang Myoun Ko, and Jong-Duk Kim. Hydrothermal preparation of nitrogen-doped graphene sheets via hexamethylenetetramine for application as supercapacitor electrodes, 2012.

[86] Seung-Bok Lee and Su-Il Pyun. The effect of electrolyte temperature on the passivity of solid electrolyte interphase formed on a graphite electrode. *Carbon N. Y.*, 40(13):2333–2339, January 2002.

[87] Dennis Y C Leung and Yuan Yang. Wind energy development and its environmental impact: A review. *Renewable Sustainable Energy Rev.*, 16(1):1031–1039, January 2012.

[88] Baojun Li, Huaqiang Cao, Jin Shao, Meizhen Qu, and Jamie H Warner. Superparamagnetic Fe3O4 nanocrystals@graphene composites for energy storage devices, 2011.

[89] Changling Li, Chueh Liu, Wei Wang, Zafer Mutlu, Jeffrey Bell, Kazi Ahmed, Rachel Ye, Mihrimah Ozkan, and Cengiz S Ozkan. Silicon derived from glass bottles as anode materials for lithium ion full cell batteries. *Sci. Rep.*, 7(1):917, April 2017.

[90] Nian-Wu Li, Ya-Xia Yin, Chun-Peng Yang, and Yu-Guo Guo. An artificial solid electrolyte interphase layer for stable lithium metal anodes. *Adv. Mater.*, 28(9):1853–1858, March 2016.

[91] Nianwu Li, Mingbo Zheng, Hongling Lu, Zibo Hu, Chenfei Shen, Xiaofeng Chang, Guangbin Ji, Jieming Cao, and Yi Shi. High-rate lithium–sulfur batteries promoted by reduced graphene oxide coating. *Chem. Commun.*, 48(34):4106–4108, March 2012.

[92] Ning Li, Qi Zhang, Song Gao, Qin Song, Rong Huang, Long Wang, Liwei Liu, Jianwu Dai, Mingliang Tang, and Guosheng Cheng. Three-dimensional graphene foam as a biocompatible and conductive scaffold for neural stem cells. *Sci. Rep.*, 3:1604, 2013.

[93] Weiyang Li, Hongbin Yao, Kai Yan, Guangyuan Zheng, Zheng Liang, Yet-Ming Chiang, and Yi Cui. The synergetic effect of lithium polysulfide and lithium nitrate to prevent lithium dendrite growth. *Nat. Commun.*, 6:7436, June 2015.

[94] Xiaolin Li, Meng Gu, Shenyang Hu, Rhiannon Kennard, Pengfei Yan, Xilin Chen, Chongmin Wang, Michael J Sailor, Ji-Guang Zhang, and Jun Liu. Mesoporous silicon sponge as an anti-pulverization structure for high-performance lithium-ion battery anodes. *Nat. Commun.*, 5:4105, July 2014.

[95] Yingru Li, Ji Chen, Liang Huang, Chun Li, Jong-Dal Hong, and Gaoquan Shi. Highly compressible macroporous graphene monoliths via an improved hydrothermal process. *Adv. Mater.*, 26(28):4789–4793, July 2014.

[96] Zhen Li, Jintao Zhang, and Xiong Wen Lou. Hollow carbon nanofibers filled with MnO2 nanosheets as efficient sulfur hosts for lithium–sulfur batteries. *Angew. Chem. Int. Ed.*, 54(44):12886–12890, 2015.

[97] Zheng Li, Zheng Liu, Haiyan Sun, and Chao Gao. Superstructured assembly of nanocarbons: Fullerenes, nanotubes, and graphene. *Chem. Rev.*, 115(15):7046–7117, August 2015.

[98] Bo Liang, Yanping Liu, and Yunhua Xu. Silicon-based materials as high capacity anodes for next generation lithium ion batteries. *J. Power Sources*, 267:469–490, December 2014.

[99] Xiao Liang, Arnd Garsuch, and Linda F Nazar. Sulfur cathodes based on conductive MXene nanosheets for High-Performance Lithium-Sulfur batteries, 2015.

[100] Xiao Liang, Connor Hart, Quan Pang, Arnd Garsuch, Thomas Weiss, and Linda F Nazar. A highly efficient polysulfide mediator for lithium–sulfur batteries, 2015.

[101] Dingchang Lin, Yayuan Liu, and Yi Cui. Reviving the lithium metal anode for high-energy batteries. *Nat. Nanotechnol.*, 12(3):194–206, March 2017.

[102] Zhan Lin, Zengcai Liu, Wujun Fu, Nancy J Dudney, and Chengdu Liang. Phosphorous pentasulfide as a novel additive for High-Performance Lithium-Sulfur batteries, 2013.

[103] Bin Liu, Ji-Guang Zhang, and Wu Xu. Advancing lithium metal batteries. *Joule*, 2(5):833–845, May 2018.

[104] Nian Liu, Liangbing Hu, Matthew T McDowell, Ariel Jackson, and Yi Cui. Prelithiated silicon nanowires as an anode for lithium ion batteries. *ACS Nano*, 5(8):6487–6493, August 2011.

[105] Nian Liu, Hui Wu, Matthew T McDowell, Yan Yao, Chongmin Wang, and Yi Cui. A yolk-shell design for stabilized and scalable li-ion battery alloy anodes. *Nano Lett.*, 12(6):3315–3321, June 2012.

[106] Qing-Chao Liu, Ji-Jing Xu, Shuang Yuan, Zhi-Wen Chang, Dan Xu, Yan-Bin Yin, Lin Li, Hai-Xia Zhong, Yin-Shan Jiang, Jun-Min Yan, and Others. Artificial protection film on lithium metal anode toward Long-Cycle-Life Lithium–Oxygen batteries. *Adv. Mater.*, 27(35):5241–5247, 2015.

[107] Languang Lu, Xuebing Han, Jianqiu Li, Jianfeng Hua, and Minggao Ouyang. A review on the key issues for lithium-ion battery management in electric vehicles. *J. Power Sources*, 226:272–288, March 2013.

[108] Songtao Lu, Yan Chen, Xiaohong Wu, Zhida Wang, and Yang Li. Three-dimensional sulfur/graphene multifunctional hybrid sponges for lithium-sulfur batteries with large areal mass loading. *Sci. Rep.*, 4:4629, April 2014.

[109] Jingshan Luo, Jilei Liu, Zhiyuan Zeng, Chi Fan Ng, Lingjie Ma, Hua Zhang, Jianyi Lin, Zexiang Shen, and Hong Jin Fan. Three-Dimensional graphene foam supported Fe3O4 lithium battery anodes with long cycle life and high rate capability. *Nano Lett.*, 13(12):6136–6143, December 2013.

[110] Zhiqiang Luo, Sanhua Lim, Zhiqun Tian, Jingzhi Shang, Linfei Lai, Brian MacDonald, Chao Fu, Zexiang Shen, Ting Yu, and Jianyi Lin. Pyridinic N doped graphene : synthesis, electronic structure, and electrocatalytic property. *J. Mater. Chem.*, 21(22):8038–8044, 2011.

[111] Arumugam Manthiram, Yongzhu Fu, and Yu-Sheng Su. Challenges and prospects of Lithium–Sulfur batteries. *Acc. Chem. Res.*, 46(5):1125–1134, May 2013.

[112] Daniela C Marcano, Dmitry V Kosynkin, Jacob M Berlin, Alexander Sinitskii, Zhengzong Sun, Alexander Slesarev, Lawrence B Alemany, Wei Lu, and James M Tour. Improved synthesis of graphene oxide. *ACS Nano*, 4(8):4806–4814, August 2010.

[113] Filippo Marchioni, Kurt Star, Erik Menke, Thierry Buffeteau, Laurent Servant, Bruce Dunn, and Fred Wudl. Protection of lithium metal surfaces using chlorosilanes. *Langmuir*, 23(23):11597–11602, November 2007.

[114] E Markevich, G Salitra, Y Talyosef, F Chesneau, and D Aurbach. Review—On the mechanism of Quasi-Solid-State lithiation of sulfur encapsulated in microporous carbons: Is the existence of small sulfur molecules necessary? *J. Electrochem. Soc.*, 164(1):A6244–A6253, January 2017.

[115] Brian Vad Mathiesen, Henrik Lund, and Kenneth Karlsson. 100% renewable energy systems, climate mitigation and economic growth. *Appl. Energy*, 88(2):488–501, February 2011.

[116] Matthew T McDowell, Seok Woo Lee, William D Nix, and Yi Cui. 25th anniversary article: understanding the lithiation of silicon and other alloying anodes for lithium-ion batteries. *Adv. Mater.*, 25(36):4966–4985, 2013.

[117] Yuriy V Mikhaylik and James R Akridge. Polysulfide shuttle study in the Li/S battery system. *J. Electrochem. Soc.*, 151(11):A1969–A1976, November 2004.

[118] Dinesh Mohan, Ankur Sarswat, Yong Sik Ok, and Charles U Pittman, Jr. Organic and inorganic contaminants removal from water with biochar, a renewable, low cost and sustainable adsorbent–a critical review. *Bioresour. Technol.*, 160:191–202, 2014.

[119] Joseph V Mullin. Continuing to improve oil spill response in the arctic: A joint industry programme. In Lawrence P Hildebrand, Lawson W Brigham, and Tafsir M Johansson, editors, *Sustainable Shipping in a Changing Arctic*, pages 335–357. Springer International Publishing, Cham, 2018.

78

[120] Lingeswarran Muniandy, Farook Adam, Abdul Rahman Mohamed, and Eng-Poh Ng. The synthesis and characterization of high purity mixed microporous/mesoporous activated carbon from rice husk using chemical activation with NaOH and KOH, 2014.

[121] Atle B Nordvik, James L Simmons, Kenneth R Bitting, Alun Lewis, and Tove Strøm-Kristiansen. Oil and water separation in marine oil spill clean-up operations. *Spill Sci. Technol. Bull.*, 3(3):107–122, January 1996.

[122] Dara O'Rourke and Sarah Connolly. JUST OIL? THE DISTRIBUTION OF ENVIRONMENTAL AND SOCIAL IMPACTS OF OIL PRODUCTION AND CONSUMPTION. *Annu. Rev. Environ. Resour.*, 28(1):587–617, November 2003.

[123] Quan Pang, Dipan Kundu, and Linda F Nazar. A graphene-like metallic cathode host for long-life and high-loading lithium–sulfur batteries. *Mater. Horiz.*, 3(2):130–136, February 2016.

[124] Quan Pang, Xiao Liang, Chun Yuen Kwok, and Linda F Nazar. Advances in lithium–sulfur batteries based on multifunctional cathodes and electrolytes. *Nature Energy*, 1:16132, September 2016.

[125] Quan Pang, Xiao Liang, Abhinandan Shyamsunder, and Linda F Nazar. An in vivo formed solid electrolyte surface layer enables stable plating of li metal. *Joule*, 1(4):871–886, December 2017.

[126] Quan Pang, Juntao Tang, He Huang, Xiao Liang, Connor Hart, Kam C Tam, and Linda F Nazar. A nitrogen and sulfur Dual-Doped carbon derived from Polyrhodanine@Cellulose for advanced Lithium-Sulfur batteries, 2015.

[127] N L Panwar, S C Kaushik, and Surendra Kothari. Role of renewable energy sources in environmental protection: A review. *Renewable Sustainable Energy Rev.*, 15(3):1513–1524, April 2011.

[128] Haesun Park, Hyun Seung Koh, and Donald J Siegel. First-Principles study of redox end members in Lithium–Sulfur batteries. *J. Phys. Chem. C*, 119(9):4675–4683, March 2015.

[129] Jun-Woo Park, Kento Yamauchi, Eriko Takashima, Naoki Tachikawa, Kazuhide Ueno, Kaoru Dokko, and Masayoshi Watanabe. Solvent effect of room temperature ionic liquids on electrochemical reactions in Lithium–Sulfur batteries. *J. Phys. Chem. C*, 117(9):4431–4440, March 2013.

[130] Min-Sik Park, Ji-Sang Yu, Ki Jae Kim, Goojin Jeong, Jae-Hun Kim, Taeeun Yim, Yong-Nam Jo, Uk Hwang, Shin Kang, Taewoo Woo, Hansu Kim, and Young-Jun Kim. Porous carbon spheres as a functional conducting framework for use in lithium–sulfur batteries, 2013.

[131] Sheng Peng and Shouheng Sun. Synthesis and characterization of monodisperse hollow Fe3O4 nanoparticles. *Angew. Chem. Int. Ed Engl.*, 46(22):4155–4158, 2007.

[132] Michael Thompson Pettes, Hengxing Ji, Rodney S Ruoff, and Li Shi. Thermal transport in three-dimensional foam architectures of few-layer graphene and ultra-thin graphite. *Nano Lett.*, 12(6):2959–2964, June 2012.

[133] Shi Qiu, Bo Jiang, Xing Zheng, Jingtang Zheng, Chaosheng Zhu, and Mingbo Wu. Hydrophobic and fire-resistant carbon monolith from melamine sponge: A recyclable sorbent for oil–water separation. *Carbon N. Y.*, 84:551–559, April 2015.

[134] Aiswarya Ragothaman and William A Anderson. Air quality impacts of petroleum refining and petrochemical industries. *Environments*, 4(3):66, September 2017.

[135] Maria Rosa Ras, Rosa Maria Marcé, and Francesc Borrull. Characterization of ozone precursor volatile organic compounds in urban atmospheres and around the petro-chemical industry in the tarragona region. *Sci. Total Environ.*, 407(14):4312–4319, July 2009.

[136] Roberto Rico-Martínez, Terry W Snell, and Tonya L Shearer. Synergistic toxicity of macondo crude oil and dispersant corexit 9500a® to the brachionus plicatilis species complex (rotifera). *Environ. Pollut.*, 173:5–10, February 2013.

[137] Calum Robertson and Robert Mokaya. Microporous activated carbon aerogels via a simple subcritical drying route for CO2 capture and hydrogen storage. *Microporous Mesoporous Mater.*, 179:151–156, September 2013.

[138] Ariel Rosenman, Elena Markevich, Gregory Salitra, Doron Aurbach, Arnd Garsuch, and Frederick Francois Chesneau. Review on li-sulfur battery systems: an integral perspective. *Advanced Energy Materials*, 5(16):1500212, 2015.

[139] Eugen Rusu and Vengatesan Venugopal. Special issue "offshore renewable energy: Ocean waves, tides and offshore wind". *Energies*, 12(1):182, January 2019.

[140] Hossein Saber, Moein Moeini-Aghtaie, Mehdi Ehsan, and Mahmud Fotuhi-Firuzabad. A scenario-based planning framework for energy storage systems with the main goal of mitigating wind curtailment issue. *Int. J. Electr. Power Energy Syst.*, 104:414–422, January 2019.

[141] Johan Scheers, Sébastien Fantini, and Patrik Johansson. A review of electrolytes for lithium–sulphur batteries. *J. Power Sources*, 255:204–218, June 2014.

[142] Bruno Scrosati. Recent advances in lithium ion battery materials. *Electrochim. Acta*, 45(15):2461–2466, May 2000.

[143] Jieqiong Shan, Yuxin Liu, Yuezeng Su, Ping Liu, Xiaodong Zhuang, Dongqing Wu, Fan Zhang, and Xinliang Feng. Graphene-directed two-dimensional porous carbon frameworks for high-performance lithium–sulfur battery cathodes. *J. Mater. Chem. A Mater. Energy Sustain.*, 4(1):314–320, 2016.

[144] Xin Shen, He Liu, Xin-Bing Cheng, Chong Yan, and Jia-Qi Huang. Beyond lithium ion batteries: Higher energy density battery systems based on lithium metal anodes. *Energy Storage Materials*, 12:161–175, May 2018.

[145] Yi Shen, Qile Fang, and Baoliang Chen. Environmental applications of three-dimensional graphene-based macrostructures: adsorption, transformation, and detection. *Environ. Sci. Technol.*, 49(1):67–84, January 2015.

[146] Zheng Shen, Lei Cao, Christopher D Rahn, and Chao-Yang Wang. Least squares galvanostatic intermittent titration technique (LS-GITT) for accurate solid phase diffusivity measurement. *J. Electrochem. Soc.*, 160(10):A1842–A1846, January 2013.

[147] K S W Sing. Reporting physisorption data for gas/solid systems with special reference to the determination of surface area and porosity (recommendations 1984), 1985.

[148] Douglas A Skoog, F James Holler, and Stanley R Crouch. *Principles of Instrumental Analysis*. Cengage Learning, January 2017.

[149] K H Solangi, M R Islam, R Saidur, N A Rahim, and H Fayaz. A review on global solar energy policy. *Renewable Sustainable Energy Rev.*, 15(4):2149–2163, May 2011.

[150] Johanna K Stark, Yi Ding, and Paul A Kohl. Nucleation of electrodeposited lithium metal: Dendritic growth and the effect of Co-Deposited sodium. *J. Electrochem. Soc.*, 160(9):D337–D342, January 2013.

[151] M Steinberg. Fossil fuel decarbonization technology for mitigating global warming. *Int. J. Hydrogen Energy*, 24(8):771–777, August 1999.

[152] Xin Su, Qingliu Wu, Juchuan Li, Xingcheng Xiao, Amber Lott, Wenquan Lu, Brian W Sheldon, and Ji Wu. Silicon-based nanomaterials for lithium-ion batteries: a review. *Advanced Energy Materials*, 4(1):1300882, 2014.

[153] Yu-Sheng Su and Arumugam Manthiram. A new approach to improve cycle performance of rechargeable lithium–sulfur batteries by inserting a free-standing MWCNT interlayer, 2012.

[154] Haiyan Sun, Zhen Xu, and Chao Gao. Multifunctional, Ultra-Flyweight, synergistically assembled carbon aerogels, 2013.

[155] J-M Tarascon, J M. Tarascon, and M Armand. Issues and challenges facing rechargeable lithium batteries, 2001.

[156] Ranganath Teki, Moni K Datta, Rahul Krishnan, Thomas C Parker, Toh-Ming Lu, Prashant N Kumta, and Nikhil Koratkar. Nanostructured silicon anodes for lithium ion rechargeable batteries. *Small*, 5(20):2236–2242, October 2009.

[157] Palanisamy Thanikaivelan, Narayanan T Narayanan, Bhabendra K Pradhan, and Pulickel M Ajayan. Collagen based magnetic nanocomposites for oil removal applications. *Sci. Rep.*, 2:230, January 2012.

[158] Rebecca S Thompson, David J Schroeder, Carmen M López, Susanna Neuhold, and John T Vaughey. Stabilization of lithium metal anodes using silane-based coatings. *Electrochem. commun.*, 13(12):1369–1372, December 2011.

[159] Yushen Tian, Siqin Xiong, Xiaoming Ma, and Junping Ji. Structural path decomposition of carbon emission: A study of china's manufacturing industry. *J. Clean. Prod.*, 193:563–574, August 2018.

[160] Grant A Umeda, Erik Menke, Monique Richard, Kimber L Stamm, Fred Wudl, and Bruce Dunn. Protection of lithium metal surfaces using tetraethoxysilane. *J. Mater. Chem.*, 21(5):1593–1599, 2011.

[161] Varun, Ravi Prakash, and Inder Krishnan Bhat. Energy, economics and environmental impacts of renewable energy systems. *Renewable Sustainable Energy Rev.*, 13(9):2716–2721, December 2009.

[162] Alexandru Vlad, Arava Leela Mohana Reddy, Anakha Ajayan, Neelam Singh, Jean-François Gohy, Sorin Melinte, and Pulickel M Ajayan. Roll up nanowire battery from silicon chips. *Proc. Natl. Acad. Sci. U. S. A.*, 109(38):15168–15173, September 2012.

[163] S Waluś, G Offer, I Hunt, Y Patel, T Stockley, and others. Volumetric expansion of Lithium-Sulfur cell during operation–fundamental insight into applicable characteristics. *Energy Storage*, 2018.

[164] Hailiang Wang, Yuan Yang, Yongye Liang, Joshua Tucker Robinson, Yanguang Li, Ariel Jackson, Yi Cui, and Hongjie Dai. Graphene-Wrapped sulfur particles as a rechargeable Lithium–Sulfur battery cathode material with high capacity and cycling stability. *Nano Lett.*, 11(7):2644–2647, July 2011.

[165] Lei Wang, Ziyue Zhou, Xiao Yan, Feng Hou, Lei Wen, Wenbin Luo, Ji Liang, and Shi Xue Dou. Engineering of lithium-metal anodes towards a safe and stable battery. *Energy Storage Materials*, 14:22–48, September 2018.

[166] Yongqiang Wang, Bingfang Zou, Tao Gao, Xiaoping Wu, Shiyun Lou, and Shaomin Zhou. Synthesis of orange-like Fe3O4/PPy composite microspheres and their excellent cr(vi) ion removal properties, 2012.

[167] M Wild, L O'Neill, T Zhang, R Purkayastha, G Minton, M Marinescu, and G J Offer. Lithium sulfur batteries, a mechanistic review. *Energy Environ. Sci.*, 8(12):3477–3494, 2015.

[168] Feixiang Wu, Jung Tae Lee, Naoki Nitta, Hyea Kim, Oleg Borodin, and Gleb Yushin. Lithium iodide as a promising electrolyte additive for Lithium-Sulfur batteries: Mechanisms of performance enhancement, 2015.

[169] Feng Wu, Yan-Xia Yuan, Xin-Bing Cheng, Ying Bai, Yu Li, Chuan Wu, and Qiang Zhang. Perspectives for restraining harsh lithium dendrite growth: Towards robust lithium metal anodes. *Energy Storage Materials*, 15:148–170, November 2018.

[170] Hui Wu, Guangyuan Zheng, Nian Liu, Thomas J Carney, Yuan Yang, and Yi Cui. Engineering empty space between si nanoparticles for lithium-ion battery anodes. *Nano Lett.*, 12(2):904–909, February 2012.

[171] Meifen Wu, Zhaoyin Wen, Yu Liu, Xiuyan Wang, and Lezhi Huang. Electrochemical behaviors of a Li3N modified li metal electrode in secondary lithium batteries. *J. Power Sources*, 196(19):8091–8097, October 2011.

[172] Wenjie Wu and Mathew M Maye. Void coalescence in core/alloy nanoparticles with stainless interfaces. *Small*, 10(2):271–276, January 2014.

[173] Yingpeng Wu, Ningbo Yi, Lu Huang, Tengfei Zhang, Shaoli Fang, Huicong Chang, Na Li, Jiyoung Oh, Jae Ah Lee, Mikhail Kozlov, Alin C Chipara, Humberto Terrones, Peishuang Xiao, Guankui Long, Yi Huang, Fan Zhang, Long Zhang, Xavier Lepró, Carter Haines, Márcio Dias Lima, Nestor Perea Lopez, Lakshmy P Rajukumar, Ana L Elias, Simin Feng, Seon Jeong Kim, N T Narayanan, Pulickel M Ajayan, Mauricio Terrones, Ali Aliev, Pengfei Chu, Zhong Zhang, Ray H Baughman, and Yongsheng Chen. Three-dimensionally bonded spongy graphene material with super compressive elasticity and near-zero poisson's ratio. *Nat. Commun.*, 6:6141, January 2015.

[174] Zhen-Yu Wu, Chao Li, Hai-Wei Liang, Yu-Ning Zhang, Xin Wang, Jia-Fu Chen, and Shu-Hong Yu. Carbon nanofiber aerogels for emergent cleanup of oil spillage and chemical leakage under harsh conditions. *Sci. Rep.*, 4:4079, February 2014.

[175] Hongfa Xiang, Pengcheng Shi, Priyanka Bhattacharya, Xilin Chen, Donghai Mei, Mark E Bowden, Jianming Zheng, Ji-Guang Zhang, and Wu Xu. Enhanced charging capability of lithium metal batteries based on lithium bis(trifluoromethanesulfonyl)imide-lithium bis(oxalato)borate dual-salt electrolytes, 2016.

[176] Lifen Xiao, Yuliang Cao, Jie Xiao, Birgit Schwenzer, Mark H Engelhard, Laxmikant V Saraf, Zimin Nie, Gregory J Exarhos, and Jun Liu. A soft approach to encapsulate sulfur: Polyaniline nanotubes for Lithium-Sulfur batteries with long cycle life, 2012.

[177] Shizhao Xiong, Kai Xie, Yan Diao, and Xiaobin Hong. Properties of surface film on lithium anode with LiNO3 as lithium salt in electrolyte solution for lithium–sulfur batteries. *Electrochim. Acta*, 83:78–86, November 2012.

[178] Shizhao Xiong, Kai Xie, Yan Diao, and Xiaobin Hong. On the role of polysulfides for a stable solid electrolyte interphase on the lithium anode cycled in lithium–sulfur batteries. *J. Power Sources*, 236:181–187, August 2013.

[179] Jiandong Xu, Qiuming Gao, Yunlu Zhang, Yanli Tan, Weiqian Tian, Lihua Zhu, and Lei Jiang. Preparing two-dimensional microporous carbon from pistachio nutshell with high areal capacitance as supercapacitor materials. *Sci. Rep.*, 4:5545, July 2014.

[180] Yuxi Xu, Kaixuan Sheng, Chun Li, and Gaoquan Shi. Self-assembled graphene hydrogel via a one-step hydrothermal process. *ACS Nano*, 4(7):4324–4330, July 2010.

[181] Yuhua Xue, Jun Liu, Hao Chen, Ruigang Wang, Dingqiang Li, Jia Qu, and Liming Dai. Nitrogen-Doped graphene foams as Metal-Free counter electrodes in High-Performance Dye-Sensitized solar cells, 2012.

[182] H Yamin, A Gorenshtein, J Penciner, Y Sternberg, and E Peled. ChemInform abstract: Lithium sulfur battery. Oxidation/Reduction mechanisms of polysulfides in THF solutions, 1988.

[183] Kai Yan, Hyun-Wook Lee, Teng Gao, Guangyuan Zheng, Hongbin Yao, Haotian Wang, Zhenda Lu, Yu Zhou, Zheng Liang, Zhongfan Liu, Steven Chu, and Yi Cui. Ultrathin two-dimensional atomic crystals as stable interfacial layer for improvement of lithium metal anode. *Nano Lett.*, 14(10):6016–6022, October 2014.

[184] Huijun Yang, Cheng Guo, Ahmad Naveed, Jingyu Lei, Jun Yang, Yanna Nuli, and Jiulin Wang. Recent progress and perspective on lithium metal anode protection. *Energy Storage Materials*, 14:199–221, September 2018.

[185] Yuan Yang, Matthew T McDowell, Ariel Jackson, Judy J Cha, Seung Sae Hong, and Yi Cui. New nanostructured Li2S/silicon rechargeable battery with high specific energy. *Nano Lett.*, 10(4):1486–1491, April 2010.

[186] Zhi-Yu Yang, Lin-Jian Jin, Guo-Qian Lu, Qing-Qing Xiao, Yu-Xia Zhang, Lin Jing, Xiao-Xue Zhang, Yi-Ming Yan, and Ke-Ning Sun. Sponge-templated preparation of high surface area graphene with ultrahigh capacitive deionization performance. *Adv. Funct. Mater.*, 24(25):3917–3925, 2014.

[187] Xi Yao, Yanlin Song, and Lei Jiang. Applications of bio-inspired special wettable surfaces. *Adv. Mater.*, 23(6):719–734, 2011.

[188] Fazel Yavari, Zongping Chen, Abhay V Thomas, Wencai Ren, Hui-Ming Cheng, and Nikhil Koratkar. High sensitivity gas detection using a macroscopic three-dimensional graphene foam network. *Sci. Rep.*, 1:166, November 2011.

[189] Rachel Ye, Jeffrey Bell, Daisy Patino, Kazi Ahmed, Mihri Ozkan, and Cengiz S Ozkan. Advanced Sulfur-Silicon full cell architecture for lithium ion batteries. *Sci. Rep.*, 7(1):17264, December 2017.

[190] Jiao Yin, Duanyi Zhang, Jiquan Zhao, Xiaolei Wang, Hui Zhu, and Chuanyi Wang. Meso- and micro- porous composite carbons derived from humic acid for supercapacitors, 2014.

[191] Ya-Xia Yin, Sen Xin, Yu-Guo Guo, and Li-Jun Wan. Lithium-sulfur batteries: electrochemistry, materials, and prospects. *Angew. Chem. Int. Ed Engl.*, 52(50):13186–13200, December 2013.

[192] Liang Zhang, Liwen Ji, Per-Anders Glans, Yuegang Zhang, Junfa Zhu, and Jinghua Guo. Electronic structure and chemical bonding of a graphene oxide–sulfur nanocomposite for use in superior performance lithium–sulfur cells. *Phys. Chem. Chem. Phys.*, 14(39):13670–13675, 2012.

[193] Sheng S Zhang. Role of LiNO3 in rechargeable lithium/sulfur battery. *Electrochim. Acta*, 70:344–348, May 2012.

[194] Sheng S Zhang. Liquid electrolyte lithium/sulfur battery: Fundamental chemistry, problems, and solutions. *J. Power Sources*, 231:153–162, June 2013.

[195] Wei-Jun Zhang. A review of the electrochemical performance of alloy anodes for lithium-ion batteries. *J. Power Sources*, 196(1):13–24, January 2011.

[196] Y J Zhang, W Wang, H Tang, W Q Bai, X Ge, X L Wang, C D Gu, and J P Tu. An ex-situ nitridation route to synthesize Li3N-modified li anodes for lithium secondary batteries. *J. Power Sources*, 277:304–311, March 2015.

[197] X Zhao, G Cheruvally, C Kim, K K Cho, H J Ahn, and others. Lithium/sulfur secondary batteries: a review. *of Electrochemical* , 2016.

[198] Yang Zhao, Chuangang Hu, Yue Hu, Huhu Cheng, Gaoquan Shi, and Liangti Qu. A versatile, ultralight, nitrogen-doped graphene framework. *Angew. Chem. Int. Ed.*, 51(45):11371–11375, 2012.

[199] Fangcai Zheng, Yang Yang, and Qianwang Chen. High lithium anodic performance of highly nitrogen-doped porous carbon prepared from a metal-organic framework. *Nat. Commun.*, 5:5261, November 2014.

[200] Guangyuan Zheng, Seok Woo Lee, Zheng Liang, Hyun-Wook Lee, Kai Yan, Hongbin Yao, Haotian Wang, Weiyang Li, Steven Chu, and Yi Cui. Interconnected hollow carbon nanospheres for stable lithium metal anodes. *Nat. Nanotechnol.*, 9(8):618–623, August 2014.

[201] Yujie Zhu and Chunsheng Wang. Galvanostatic intermittent titration technique for Phase-Transformation electrodes. *J. Phys. Chem. C*, 114(6):2830–2841, February 2010.